



ORIGINAL ARTICLE

Rescue of p53 functions by in vitro-transcribed mRNA impedes the growth of high-grade serous ovarian cancer

Monika Raab¹ | Izabela Kostova¹ | Samuel Peña-Llopis^{2,3,4}  | Daniela Fietz⁵ |
 Monika Kressin^{1,5} | Seyed Mohsen Aberoumandi^{5,6,7} | Evelyn Ullrich^{6,7,8} |
 Sven Becker¹ | Mourad Sanhaji¹ | Klaus Strebhardt^{1,4} 

¹Department of Gynecology, Medical School, Goethe-University, Frankfurt am Main, Germany

²Translational Genomics in Solid Tumors, West German Cancer Center, University Hospital, Essen, Germany

³German Cancer Consortium (DKTK), Essen, Germany

⁴German Cancer Research Center (DKFZ), Heidelberg, Germany

⁵Histology and Embryology, Institute for Veterinary Anatomy, Giessen, Germany

⁶Franfurt Cancer Institute (FCI), Goethe University, Frankfurt am Main, Germany

⁷German Cancer Consortium (DKTK), Partner site Frankfurt/Mainz, a partnership between DKFZ and University Hospital Frankfurt, Frankfurt am Main, Germany

⁸Experimental Immunology, Department for Children and Adolescents Medicine, University Hospital Frankfurt, Goethe University, Frankfurt am Main, Germany

Correspondence

Klaus Strebhardt and Mourad Sanhaji,
 Department of Gynecology, Medical
 School, Goethe-University, 60590
 Theodor-Stern-Kai 7-9, Frankfurt am
 Main, Germany.
 Email: strebhardt@em.uni-frankfurt.de;
Mourad.Sanhaji@kgu.de

Funding information

Deutsche Krebshilfe, Grant/Award
 Number: 70114007; Wilhelm Sander
 Stiftung, Grant/Award Number:
 2021.023.1

Abstract

Background: The cellular tumor protein p53 (*TP53*) is a tumor suppressor gene that is frequently mutated in human cancers. Among various cancer types, the very aggressive high-grade serous ovarian carcinoma (HGSOC) exhibits the highest prevalence of *TP53* mutations, present in >96% of cases. Despite intensive efforts to reactivate p53, no clinical drug has been approved to rescue p53 function. In this study, our primary objective was to administer in vitro-transcribed (IVT) wild-type (WT) p53-mRNA to HGSOC cell lines, primary cells, and orthotopic mouse models, with the aim of exploring its impact on inhibiting tumor growth and dissemination, both in vitro and in vivo.

Methods: To restore the activity of p53, WT p53 was exogenously expressed in HGSOC cell lines using a mammalian vector system. Moreover, IVT WT p53 mRNA was delivered into different HGSOC model systems (primary cells and patient-derived organoids) using liposomes and studied for proliferation,

List of abbreviations: APC, Adenomatous polyposis coli protein; BAK, B-cell lymphoma 2 (BCL-2) antagonist/killer; BAX, BCL-2 associated X-protein; BCL-2, B-cell lymphoma 2; Bid, BH3 interacting domain death agonist; Bub1, Mitotic checkpoint serine/threonine kinase; BUB1B, BUB1 mitotic checkpoint serine/threonine kinase B; CDC20, Cell division protein 20 homolog; CDK1, Cyclin-dependent Kinase 1; EGFP, Enhanced Green Fluorescence Protein; FAS, Tumor necrosis factor receptor superfamily member 6; GSK3 β , Glycogen synthase kinase 3 β ; H2AX, H2A histone family member X; HGSOC, high-grade serous ovarian cancer; IVT, in vitro transcription; MDM2, Double minute 2 homolog protein; MYC, Master regulator of cell cycle entry and proliferative metabolism; Noxa, NADPH oxidase activator 1; p14ARF, ARF tumor suppressor; p16, inhibitor of cyclin-dependent kinase 4 (CDK4) and CDK6; P21/(*CDKN1A*), Cyclin-dependent kinase inhibitor 1; p27, Inhibitor of cyclin-dependent kinase 4 (CDK4) and CDK6; PARP, Poly (ADP-ribose) polymerase; PLK1, Polo-like Kinase 1; PLK3, Polo-like Kinase 3; Puma, The p53 upregulated modulator of apoptosis; *TP53*, Tumor Protein p53; XIAP, X-linked inhibitor of apoptosis.

This is an open access article under the terms of the [Creative Commons Attribution-NonCommercial-NoDerivs](https://creativecommons.org/licenses/by-nc-nd/4.0/) License, which permits use and distribution in any medium, provided the original work is properly cited, the use is non-commercial and no modifications or adaptations are made.

© 2023 The Authors. *Cancer Communications* published by John Wiley & Sons Australia, Ltd. on behalf of Sun Yat-sen University Cancer Center.

cell cycle progression, apoptosis, colony formation, and chromosomal instability. Transcriptomic alterations induced by p53 mRNA were analyzed using RNA sequencing in OVCAR-8 and primary HGSOC cells, followed by ingenuity pathway analysis. In vivo effects on tumor growth and metastasis were studied using orthotopic xenografts and metastatic intraperitoneal mouse models.

Results: Reactivation of the *TP53* tumor suppressor gene was explored in different HGSOC model systems using newly designed IVT mRNA-based methods. The introduction of WT p53 mRNA triggered dose-dependent apoptosis, cell cycle arrest, and potent long-lasting inhibition of HGSOC cell proliferation. Transcriptome analysis of OVCAR-8 cells upon mRNA-based p53 reactivation revealed significant alterations in gene expression related to p53 signaling, such as apoptosis, cell cycle regulation, and DNA damage. Restoring p53 function concurrently reduces chromosomal instability within the HGSOC cells, underscoring its crucial contribution in safeguarding genomic integrity by moderating the baseline occurrence of double-strand breaks arising from replication stress. Furthermore, in various mouse models, treatment with p53 mRNA reduced tumor growth and inhibited tumor cell dissemination in the peritoneal cavity in a dose-dependent manner.

Conclusions: The IVT mRNA-based reactivation of p53 holds promise as a potential therapeutic strategy for HGSOC, providing valuable insights into the molecular mechanisms underlying p53 function and its relevance in ovarian cancer treatment.

KEYWORDS

apoptosis, cell cycle, chromosomal instability, HGSOC metastatic intraperitoneal mouse model, HGSOC orthotopic Xenograft model, high-grade serous ovarian cancer, in vitro-transcribed p53-mRNA, liposomal IVT mRNA delivery system, patient-derived organoid, patient-derived primary cancer cell

1 | BACKGROUND

High-grade serous ovarian cancer (HGSOC) is the most lethal gynecological malignancy. It interacts intensively with the tumor stroma, grows rapidly, metastasizes extensively, and shows an aggressive course [1, 2]. Ovarian cancer (OC) cells remain within the peritoneal cavity and disseminate only to the mesothelium-lined surface [3]. The current standard of care includes cytoreductive surgery, chemotherapy (platinum compounds, paclitaxel [4], and cyclophosphamide [5]), bevacizumab (avastin) [6], and poly-ADP-ribose polymerase (PARP) inhibitors [7]. Nevertheless, approximately 70% of patients experience relapse within 3 years following surgery and platinum-based chemotherapy and succumb to disease progression [8].

The tumor protein p53 (*TP53*) gene is the most frequently mutated human tumor suppressor gene, mostly through point mutations, whereby amino acid substitutions lead to the disruption of tumor protein p53 binding

to DNA [9–11]. Thus, p53 protects the human genome by counteracting cellular stress and DNA damage [12]. Multiple reports have shown that tumor cells harboring functionally inactive p53 are resistant to chemotherapeutics because their mechanism of action involves DNA damage, leading to the activation of wild-type (WT) p53. The Cancer Genome Atlas Research Network revealed that HGSOC is characterized by inactive or truncated *TP53* in up to 96% of all cases [13]. Moreover, mutations in *TP53* seem to be early events in tumorigenesis, likely in OC precursor lesions, supporting the importance of mutated *TP53* as a driver of this malignancy [14].

Approaches aimed at re-establishing the WT function of p53 have the unique ability to improve outcomes in patients with many types of cancer. Several small molecules have been developed to counteract the loss of p53 function, mostly by stabilizing the native conformation of p53 [15, 16], like PRIMA-1, which reactivates mutant p53, induces apoptosis in cancer cells [15, 17],

and is currently in clinical trials (ClinicalTrials.gov). In our laboratory, silencing of Cyclin B1 upregulated the ARF tumor suppressor, p14ARF, which inhibits mouse double minute 2 homolog protein (MDM2) and reduces p53-S315 phosphorylation by Cyclin-dependent kinase 1 (CDK1)/Cyclin B1, thereby modulating two mechanisms that stabilize and activate p53 [18]. Other small molecules have been developed to reinstate specific p53 functions [15, 19, 20], or nonsense mutations by promoting transcriptional readthrough [21]. Nevertheless, different studies have provided evidence of off-target effects associated with small molecules used for p53 reactivation [22–24]. Thus, whether off-target activities or restoration of p53 function are the origin of therapeutic responses is currently being investigated.

With benefits such as scalable manufacturing, few adverse effects, and high efficiency [25, 26], novel strategies based on mRNA therapeutics have emerged as effective and safe approaches for fighting predominantly infectious diseases. Although mRNA therapies for protein replacement are gaining attention in several clinical settings, their use in cancer remains limited [27, 28]. To explore whether mutant *TP53*-bearing HGSOC cells respond to p53 rescue, we tested an in vitro transcribed (IVT), codon-optimized p53-mRNA in human and murine models and achieved robust and persistent protein expression using diverse IVT-mRNAs. We aimed to investigate the impact of prolonged p53-mRNA treatment on the induction of cell cycle arrest, apoptosis, and chromosomal stability in HGSOC, a tumor type characterized by *TP53* loss and chromosomal instability [29]. Finally, we assessed the ability of p53-mRNA to inhibit tumor cell proliferation and dissemination in xenograft models, highlighting its potential for HGSOC therapy.

2 | MATERIALS AND METHODS

2.1 | Generation of mRNA

Plasmid templates containing open reading frames of Enhanced Green Fluorescent Protein (EGFP), luciferase, or Flag-p53 were amplified using PCR, restoring functionality to the T7 promoter sequence and adding a 120A tail via the reverse primer. The primer pair used for cloning *TP53* into Flag vector are: 5'-ATGGAGGAGCCGAGTCAGATCC-3', forward primer; 5'-TCAGTCTGAGTCAGGCCCTTCTG-3', reverse primer. These constructs were capped (Cap 1) using CleanCap® AG (Tebu-Bio, Offenbach, Hessen, Germany) in a reaction where uridine-5'-triphosphate was fully substituted with Pseudo-U. After the IVT, DNase (Tebu-Bio, Offenbach, Hessen, Germany) was used to remove any residual DNA

template from the reaction. Thorough purification of mRNAs included the use of DNase to degrade the DNA template and a spin column (silica membrane; Tebu-Bio, Offenbach, Hessen, Germany) to remove the digested template, excess nucleoside triphosphates (NTPs), salts, and unused capping analogs. A Qiagen RNeasy (silica membrane) spin column was used to remove the digested template, excess NTPs, salts, and unused capping analogs. Antarctic phosphatase (Tebu-Bio, Offenbach, Hessen, Germany) was then used to cleave residual immunogenic 5' triphosphate from any uncapped material. A second RNeasy spin column was used to remove phosphatase from the reaction. Purified mRNA was purchased from TriLink (Tebu-Bio).

2.2 | Patients and tissue samples

This study was conducted according to the “REporting recommendations for tumor MARKer prognostic studies” [30]. Following the acquisition of informed consent, samples of ovarian carcinoma were obtained from individuals diagnosed with epithelial ovarian cancer at the Department of Gynecology at Goethe University Hospital in Frankfurt am Main, Germany from January 2015 to December 2022. The validation of these samples involved assessment by 3 pathologists, with exclusion criteria applied to patients with alternative tumor types. To establish primary patient-derived OC cell cultures, we analyzed samples from 8 patients who underwent surgical resection (Supplementary Table S1). Sufficient archival materials for cell culture analyses were available for samples with validated diagnoses. The local research ethics committee approved the studies on human tissue (permit number: SGO-1-2017), and the samples were processed anonymously. The assessment of progression-free survival (PFS) extended from the surgical procedure to the point of disease relapse or progression. Cases with a PFS duration of fewer than 6 months were designated as chemoresistant, whereas durations surpassing this threshold were characterized as chemosensitive.

2.3 | Cell lines, primary cells, and transfection

Human ovarian cancer cell lines SKOV3, OVCAR-3, OVCAR-4, OVCAR-5, and OVCAR-8 were purchased from the DCTD Tumor Repository (Bethesda, MD, USA), maintained in RPMI 1640 medium (Thermo Fisher Scientific, Dreieich, Hessen, Germany), containing 10% fetal bovine serum (FBS; Thermo Fisher Scientific) and 1% penicillin-streptomycin (#17060063, Thermo Fisher Scientific). All

cell lines were cultured in a humidified incubator of 5% CO₂ at 37°C.

Primary cells were isolated from OC tissues derived from in-house surgery using a tumor dissociation (Max Miltenyi 130-095-929, Bergisch Gladbach, NRW Germany) and tumor cell isolation (Max Miltenyi 130-108-339) kits, according to the manufacturer's instructions. Briefly, the samples were stored in a solution comprising Advanced DMEM/F12 (Thermo Fisher Scientific), 2 mmol/L HEPES (Thermo Fisher Scientific), 1 × GlutaMAX-I (Thermo Fisher Scientific), and 200 U/mL penicillin/streptomycin (Thermo Fisher Scientific). Upon arrival at the laboratory, the tissue specimens were put in a sterile petri dish on ice. Following this, the tumor was cut into a sterile 10 mm square. A section of the dissected tissue was stored at −80°C in 2 mL tubes using Recovery Cell Culture Freezing Medium (Thermo Fisher Scientific) for subsequent utilization. In the process of preparing organoids, tissue samples were collected in 50 mL tubes with HBSS 1 × (Thermo Fisher Scientific) and incubated on ice for 5 minutes.

We performed DNA transfections using jetPEI Transfection Reagent (Polyplus, Illkirch, Bas-rhin, France) or LTX (Invitrogen, Waltham, MA, USA) (1 µg IVT mRNA: 2 µL Lipofectamine Messenger MAX Transfection Reagent [Invitrogen]), according to the previously described [31]. mRNA transfections were performed using the Lipofectamine Messenger MAX Transfection Reagent (Invitrogen), according to the manufacturer's instructions. Ovarian cancer cells were obtained by cell scraper and then lysed in radioimmunoprecipitation assay, RIPA buffer (Waltham, MA, USA). After centrifuging for 5 min at 15,000 ×g at 4°C, cytoplasmic protein was collected in the supernatant.

2.4 | Colony formation assay

Two thousand cells were seeded into 6-well plates. The transfected cells were washed and incubated in fresh medium for 2 weeks. The colonies were fixed using 70% ethanol and stained with 0.5 µg Coomassie Brilliant Blue (Biorad, Feldkirchen, Bavaria, Germany). The number of grown colonies was counted, and images were captured using an AxioObserver Z1 microscope (Zeiss, Göttingen, Lower Saxony, Germany) and ChemiDoc MP system (BioRad, Hercules, CA, USA).

2.5 | Organoids

Following the in-house surgery, tissues were collected in a storage medium (Dulbecco's Modified Eagle's Medium [DMEM; Thermo Fisher Scientific, 1% penicillin-

streptomycin [Thermo Fisher Scientific]) on ice and processed immediately. Fresh tissues were cut into small pieces (2-4 mm) and rinsed 3 times with wash medium (500 mL DMEM, 1% penicillin-streptomycin, and 2 g bovine serum albumin [BSA; Thermo Fisher Scientific]). Subsequently, the sample was left on ice for 2 min to settle, and the supernatant was removed. Finally, the tissue was kept in 5-20 mL digestion medium (20 mL Advanced DMEM, 20 g BSA, and 10 µmol/L Y-27632), depending on the sample size, for up to 30 min at 37°C. Every 5-10 min, the sample was shaken and the stage of digestion was examined under a microscope. The digestion process was terminated with an equal volume of wash medium, as soon as the tissue was digested into single cells or small cell clusters. After that, the cell suspension was filtered through a 100 µm-filter and spun down at 200 × g for 5 min at 4°C, and the supernatant was then removed. Red blood cells as components of the pellet were lysed with ammonium-chloride-potassium buffer (Red lysis buffer: 0.15 M NH₄Cl, 10 mmol/L KHCO₃, and 0.1 mmol/L ethylenediaminetetraacetic acid) for 2-3 min at room temperature and transferred to an Eppendorf tube. After a second wash step (200 × g, 5 min, 4°C), the pellet was resuspended in a wash medium (#356231, Corning, Kaiserslautern, NRW, Germany) and mixed with a triple volume Base Membrane Extract (BME; cat. # BME 001-05, Cultrex UltiMatrix Reduced Growth Factor Basement Membrane Extract, R+D Systems, Wiesbaden, Hessen, Germany), or Corning Matrigel. Finally, 3D drops of the mixture (10-20 µL) were seeded on a 12-well suspension plate. The plate was flipped upside down and incubated in a cell culture incubator for 30 min at 37°C, 5% CO₂. Finally, 1 mL growth medium (38.65 mL Advanced DMEM/F12 [Thermo Fischer, Dreieich, Hessen, Germany], 10 µmol/L Y-27632 [Biozol, Eching, Bavaria, Germany], 0.25 µmol/L A83-01 [Tocris, Bristol, Somerset, UK], 1 mL 1 × B27 supplement, 5 mmol/L Nicotinamide [Sigma, Frankfurt, Hessen, Germany], 1.25 mmol/L N-acetylcysteine [Sigma], 50 ng/mL human Epidermal Growth Factor [Peprotech, Cranbury, NJ, USA], 50 ng/mL Neuregulin [Peprotech], 5 ng/mL FGF-Basic [Peprotech, Cranbury, NJ, USA], 10 ng/mL hFGF-10 [Peprotech], 200 ng/mL primocin [InvivoGen, San Diego, CA, USA], 50 ng/mL R-Spondin [Peprotech], and 100 ng/mL Noggin [R&D system, Mineapolis, MN, USA]), were added to each well. The medium was replaced twice weekly. The organoids were passaged according to their size and density.

2.6 | Western blot (WB) and antibodies

Cell protein extracts were prepared by lysis in the RIPA buffer (Sigma) supplemented with protease inhibitors

(complete protease inhibitor cocktail, Roche, Mannheim, Rheinland Pfalz Germany). Protein extracts (25 μ g) were separated using sodium dodecyl sulfate-polyacrylamide gel electrophoresis and transferred onto polyvinylidene difluoride membranes using a TransBlot Turbo Transfer System (Bio-Rad, Feldkirchen, Bavaria, Germany). The membranes were blocked with tris-buffered saline with 0.05% Tween[®] 20 (Sigma, Frankfurt, Hesen, Germany) containing 2% BSA Thermo Fisher Scientific.

The following antibodies were used at the indicated concentrations: mouse monoclonal Plk1 (F-8:sc-17783) (1:1000; Santa Cruz, Biotechnology Heidelberg, Germany), GFP (B-2) (1:1000; Santa Cruz), Cyclin A (H-432) (1:1000; Santa Cruz), CDK1 (sc-54) (1:1000; Santa Cruz), KIF4A (sc-365144) (1:1000; Santa Cruz), c-Myc (sc-764) (1:1000; Santa Cruz), p53 (sc-126) (1:1000; Santa Cruz), p73 (sc-17823) (1:1000; Santa Cruz), MDM2 (sc-965) (1:1000; Santa Cruz), H-Ras (sc-30) (1:1000; Santa Cruz), Luciferase-HRP (sc-57604) (1:100; Santa Cruz), K-Ras (sc-30) (1:1000; Santa Cruz), CDK4 (sc-260; Santa Cruz), BRCA-2 (sc-293185) (1:1000; Santa Cruz), β -Actin (AC-15:A1978) (1:200; Sigma-Aldrich, Taufkirchen, Germany), Flag (M2:A8592) (1:1000; Sigma-Aldrich), PLK1 (35-206, #05-844) (1:1000; Millipore, Schwalbach, Germany), Cyclin B1 (#4138) (1:1000; Millipore), Aurora B (#3094) (1:1000; Millipore), GAPDH (ab 9485) (1:1000; Abcam, Cambridge, Cambridgeshire, England), Bak (ab 32371) (1:1000; Abcam), XIAP (ab 28151) (1:1000; Abcam), Aurora A (#14475) (1:1000; Cell Signaling, Frankfurt, Hessen, Germany), Cyclin E (#4129) (1:1000; Cell Signaling), p53-pS20 (#9287) (1:1000; Cell Signaling), p21 (#2947) (1:1000; Cell Signaling), p27 (#3686) (1:1000; Cell Signaling), p16 (#18769) (1:1000; Cell Signaling), PARP (#9542) (1:1000; Cell Signaling), Casp.3 (#9665) (1:1000; Cell Signaling), Puma (#98672) (1:1000; Cell Signaling), Noxa (#14766) (1:1000; Cell Signaling), Fas (#8023) (1:1000; Cell Signaling), TOP2A (#12286) (1:1000; Cell Signaling), BIRC5 (#2802) (1:1000; Cell Signaling), Nup98 (#2598) (1:1000; Cell Signaling), BID (#2002) (1:1000; Cell Signaling), PLK3 (#4896) (1:1000; Cell Signaling), Casp.9 (#65832) (1:1000; Cell Signaling), Bub1 (#4116) (1:1000; Cell Signaling), cdc25c (#4688) (1:1000; Cell Signaling), AKT3 (#14982) (1:1000; Cell Signaling), Cyclin D (#55506) (1:1000; Cell Signaling), GSKB (#12456) (1:1000; Cell Signaling), pGSK3B(Ser9) (#5558) (1:1000; Cell Signaling), β -Catenin (#8480) (1:1000; Cell Signaling), p- β -Catenin(S33/37/T41) (#9561) (1:1000; Cell Signaling), Bub1B (A300-386A) (1:1000; Biomol GmbH, Hamburg, Germany), cdc20 (Ls-C357796) (1:1000; Biozol), Bcl-2 (#610538) (1:1000; BD Biosciences, Heidelberg, Germany), Bax (AF 820) (1:1000; R&D, Abingdon, Oxfordshire, UK), and HRP-conjugated secondary antibodies (1:5000; GE

Healthcare and Jackson Laboratory, Bar Harbor, ME, USA. The ECL WB Substrate (Millipore) was used for detection.

2.7 | Cell cycle, cell viability, and proliferation assays

For cell cycle analysis, cells were harvested, washed with phosphate-buffered saline (PBS), fixed in chilled 70% ethanol at 4°C for 30 min, treated with 1 mg/mL RNase A (Sigma-Aldrich), and stained with 100 μ g/mL propidium iodine for 30 min. Cell cycle quantification was performed using a FACSCalibur instrument and CellQuest Pro software (both BD Biosciences).

The Caspase-Glo 3/7 assay kit (Promega, Waldorf, Hesen, Germany) was used according to the manufacturer's instructions. The measured luminescence (RLU) was presented as the mean value \pm standard deviation ($n = 3$). Apoptotic loss of membrane asymmetry was analyzed by staining with PE Annexin V and 7-AAD (BD Biosciences) and quantified using a FACSCalibur instrument. For the apoptosis assays, non-synchronized cells were treated with the test compounds for the indicated times. Cell viability assays were conducted with the Cell Titer-Blue[®] Cell Viability assay (Promega) using fluorescence as a read-out, according to the manufacturer's instructions (excitation/emission wavelengths: 562 nm/615 nm). The significance of differences between populations of data was assessed using the Student's two-tailed test (* $P \leq 0.05$; ** $P \leq 0.01$; *** $P \leq 0.001$). Proliferation assays were conducted using the Cell Titer-Blue[®] Cell Viability assay (Promega), as described [32]. In brief, cells were seeded in 96-well plates and transfected with P53-mRNA or control mRNA. After, the fluorescence was measured at the indicated time points using a Victor X4 Multilabel Counter (Victor X4, PerkinElmer, Rodgau, Hessen, Germany).

2.8 | Luciferase assay

Luciferase assays were performed using the Luciferase Assay System (Promega). Briefly, the organoids were harvested and dissociated into single cells using TrypLE and mechanical dispersion. Luciferase activity in the cells was measured according to the manufacturer's instructions. Briefly, the cells were lysed in lysis buffer. Afterwards, 20 μ L cell lysate were mixed with 100 μ L luciferase assay reagent (Promega, Waldorf, Hessen, Germany) and the luminescence was immediately recorded using a plate-reading luminometer (Victor X4, PerkinElmer, Rodgau, Germany).

2.9 | Lactate dehydrogenase (LDH) cytotoxic assay

The cell culture medium was collected and diluted (1:100) in an LDH storage buffer (Promega, Waldorf, Hessen, Germany). For a single reaction, 50 μ L of diluted cell culture medium was mixed with 50 μ L of LDH Detection Enzyme Mix (Promega) and 0.25 μ L of reductase substrate (Promega). After a 60-min incubation period at room temperature, luminescence was recorded using a plate-reading luminometer (Victor X4, PerkinElmer, Rodgau, Germany).

2.10 | Chromosome spreads

The cells were treated overnight with 3.3 μ mol/L Nocodazol (Sigma Aldrich). The next day, the cells were harvested by mitotic shake off and hypotonically swollen in 40% medium/60% tap water for 20 min at 37°C. The cells were fixed with freshly prepared Carnoy's solution (75% methanol and 25% acetic acid), and the fixative was changed several times. For spreading, the cells in Carnoy's solution were dropped onto pre-chilled glass slides. Slides were dried at room temperature for 24 h and stained with 4',6-diamidino-2-phenylindole (Thermo Fisher Scientific). Chromosome number per condition was counted using an AxioObserver.Z1 microscope with an HCX PL APO CS 63.0 \times 1.4 oil UV objective (Zeiss). Graphic representation of the results was performed using GraphPad Prism software (GraphPad.com).

2.11 | RNA sequencing (RNA-seq)

The RNA samples were used for library preparation using the NEBNext Ultra RNA Library Prep Kit (Illumina, San Diego, CA, USA). Indices were included for multiple samples. Briefly, mRNA was purified from the total RNA using poly T oligo-attached magnetic beads (Thermo Fisher Scientific). After fragmentation, first-strand cDNA was synthesized using random hexamer primers (Thermo Fisher Scientific), followed by second-strand cDNA synthesis. The library was prepared by end-repair, A-tailing, adapter ligation, and size selection. After amplification and purification, insert size of the library was validated using Agilent 2100 (Agilent, Santa Clara, CA, USA) and quantified using quantitative PCR (qPCR). Libraries were then sequenced on an Illumina NovaSeq 6000 S4flow cell with PE150, according to the results of library quality control and expected data volume.

Gene expression data were analyzed as previously reported [33]. Briefly, unpaired *t*-tests were performed

between cells transfected with p53-mRNA and the EGFP control, considering group variances. A 2-tailed Student's *t*-test was performed for equal variances or Welch's test was used for unequal variances. All calculated *P*-values were adjusted using the Benjamini and Hochberg false discovery rate (FDR) method to account for the possibility of false-positive results due to multiple tests. Genes with an FDR $q < 0.05$ and an absolute fold change (FC) > 1.5 were further analyzed using Ingenuity Pathway Analysis (IPA) software (Qiagen, Hilden, Bavaria, Germany) to identify overrepresented canonical pathways. Heatmaps of RNA-seq data were normalized to z-score by subtracting the mean from each value and dividing by the standard deviation.

2.12 | TCF/LEF reporter assay

The TCF/LEF reporter assay was purchased from BPS Bioscience (#60500) (San Diego, CA, USA) and performed according to the manufacturer's instructions. Briefly, cells were seeded in a 96-well plate one day prior to transfection to achieve a cellular confluence of 90% on the day of the transfection. The following day, a transfection mixture, consisting of Lipofectamine Messenger MAX Transfection Reagent (1 μ L of the TCF/LEF reporter plasmid) and 1 μ g of IVT mRNA, was prepared for each well. After a 25-min incubation period at room temperature, the mixture was introduced into the cells. Subsequently, a 24-h incubation at 37°C was carried out, and a dual luciferase assay was conducted using a plate-reading luminometer (Victor X4, PerkinElmer, Rodgau, Hessen, Germany) to record the assay results.

2.13 | Animal experiments

All animal experiments were approved by the regional council of Darmstadt and performed under the supervision of the Division of Laboratory Animal Medicine (Goethe University, Medical School, and Georg-Speyer-Haus). For the OC orthotopic mouse model, 6-8-week-old female nude mice (body weight: 25-30 g) were purchased from Charles River Laboratories (Sulzfeld, Bavaria, Germany) and housed under a 12 h-light/dark schedule. Twenty minutes before the surgery, the mice received analgesia (butorphanol 3 mg/kg and carprofen 2 mg/kg, subcutaneously), were kept under isoflurane anesthesia, transferred onto a heating pad to prevent hypothermia, inspected with the dorsal side up under a microscope, and kept anesthetized during the whole procedure. To confirm that the animals were under deep anesthesia,

the toes of the hind paws were pinched using forceps. The procedure was performed in the absence of a pedal reflex. The eyes were covered with ointment to avoid drying.

The optimal point of incision to reach the ovary was located on the dorsal side, to the right of the middle, and under the ribs. The area was disinfected with 70% ethanol, anesthetic skin was then gently lifted using forceps and cut into pieces. The skin was separated from the abdominal wall using blunt-ended scissors. Subsequently, the abdominal wall was cut, and the abdominal cavity was opened. The ovarian fat pad was visible adjacent to the ovary and oviduct under the microscope. The fat pad was gently pulled out of the abdominal cavity with forceps, placed on a sterile gauze, soaked in saline, and held with forceps to maintain a stable position. Approximately 1×10^6 Luc-OVCAR-8 cells were resuspended in 5 μ L PBS containing 2% Matrigel and injected into the space between the bursa and ovary with a Hamilton 10 μ L-syringe (30 G needle). Once the needle was inserted into the bursa, a second person pushed the plunger, while the surgeon maintained the correct position of the needle under a microscope. While injecting the cell suspension, expansion of the bursa was observed, indicating that the tumor cells remained in the space between the bursa and ovary. The ovarian fat pad was then placed back into the abdominal cavity. Finally, both sites of the abdominal wall were gently placed together, and the skin was closed with wound clips. On days one and two after the surgery, the animals received analgesia (butorphanol 3 mg/kg and carprofen 2 mg/kg, subcutaneously). One week after the surgery, the wound clamps were removed. The surgery was associated with minimal pain, stress, and harm to the animals. All the mice survived the surgery and showed no behavioral abnormalities after the procedure. For the intraperitoneal OC, 6-8-week-old female nude mice (body weight: 22-28 g) were used. The injection area was disinfected with 70% ethanol. The skin was gently lifted with forceps, and 2×10^6 OVCAR-8 cells were injected.

2.14 | In vivo imaging system (IVIS)

IVIS or bioluminescence imaging (BLI) was applied to monitor tumor growth and metastases. The mice were anesthetized with isoflurane. Approximately 100 μ L of luciferin (Promega, Waldorf, Hessen, Germany) was administered subcutaneously 15 min before measuring the bioluminescence. Emission of light signals was determined using an IVIS Lumina II Multispectral Imaging System (PerkinElmer, Rodgau, Hessen, Germany) [34]. The first measurement was performed on the day of cell

injection, followed by a second imaging seven days after the surgery. Thereafter, imaging was performed once a week.

2.15 | Tissue processing for anatomical and histological examination

For gross anatomical evaluation of the control and treated mice, the animals were anesthetized using isoflurane gas, injected with 100 μ L luciferin, and kept in an isoflurane chamber for 15 min to allow the luciferin to dissociate in the organs. The animals were sacrificed by cervical dislocation, placed in dorsal recumbency, and fixed with needle pins. The skin and body walls were opened at the linea alba, and pictures of each animal's body cavities were taken. Subsequently, gross macroscopic analyses of the liver, kidneys, uterus and ovaries, spleen, omentum, small and large intestines, lungs, and peritoneal surfaces were performed. Noticeable changes in organ morphology have also been previously reported. The organs and structures were excised and placed in six-well plates (all the organs except the intestine) or Petri dishes (small and large intestines) filled with PBS to keep the organs moist. IVIS measurements were performed, and all the organs were kept in PBS-buffered formalin for histological and immunohistochemical analyses or on dry ice for further molecular analyses.

Whole ovaries, including the ovarian bursa, and samples from the liver, spleen, lungs, and kidneys were carefully dissected. Intestinal tissue preparation and Swiss rolling of the small intestine and colon were performed as described [35]. The specimens were fixed in 10% neutral-buffered formalin for 48 h at room temperature. The formalin was removed by repeated washing with PBS. After dehydration in graded ethanol and exchange of ethanol with Xylol, the tissues were infiltrated with paraffin and embedded in blocks. Further, 5 μ m sections taken from different parts of the blocks were stained with hematoxylin/eosin and microscopically evaluated with respect to overall organ histology and the presence of tumors.

2.16 | Statistical methods

All experiments were performed at least in triplicates. Standardization and statistical analysis were performed as previously described [36]. Statistical analyses were performed using Microsoft Excel and GraphPad Prism. For paired t-tests, all experimental groups were compared with their respective groups. The Student's t-test and Wilcoxon test were used to determine statistical significance between

two groups, unless otherwise indicated. P value < 0.05 was considered statistically different. Significant differences ($*P \leq 0.05$, $**P \leq 0.01$, and $***P \leq 0.001$) are indicated by asterisks.

3 | RESULTS

3.1 | Mammalian vector-based expression of p53 induced apoptosis in HGSOC cells

As no sufficiently specific drug is available to rescue functional WT p53 in cancer cells bearing a loss-of-function p53 mutant, we considered reactivating the p53 gene using different experimental strategies in HGSOC cell lines and primary OC cells. First, 5 known OC cell lines were studied for p53 expression (Supplementary Figure S1A). The expression of p53 was not detected in SKOV3 or OVCAR-5 cells, in line with previous observations that classified them as p53 null [37] (Supplementary Figure S1A). In contrast, OVCAR-3, -4, and -8 cells showed abundant p53 protein expression and low to undetectable levels of the classical p53-target gene, p21. This was due to mutations within the DNA-binding domain at R248Q and L130V or a single-nucleotide mutation at the splice junction (c.376-1G > A) [38–40], which inhibited the expression of the major negative p53 regulator, MDM2 [41], within a negative feedback loop. For further analysis, we selected different HGSOC cell lines, including OVCAR-8 [42], which harbor different genomic alterations that were confirmed by sequencing (Supplementary Figure S1B). Exogenous expression of Flag-tagged WT p53 driven by a mammalian vector system for 48 h in mutant *TP53*-bearing OVCAR-8 cells significantly reduced cell proliferation compared to that in the controls (Supplementary Figure S1C). We examined cells transfected with increasing amounts of the WT p53-expressing vector (Supplementary Figure S1D) by FACS 24 h after transfection and observed a moderate increase in the percentage of apoptotic cells in the sub-G1 phase (Supplementary Figure S1E), accompanied by increased levels of caspase 3/7 activity and annexin staining (Supplementary Figure S1F). Western blot experiments for the detection of cleaved caspase-3 and PARP corroborated increasing apoptosis (Supplementary Figure S1D). To further assess the cell cycle progression, in the WB experiments, we observed an upregulation of CDK inhibitors (p16 and p27) and p21 upon a vector-prone increase of p53 expression (Supplementary Figure S1D). The expression of PLK1 and CDK1, two key players in cell cycle regulation, was reduced at higher amounts of transfected p53-mRNA likely due to increased apoptosis (Supplementary Figure

S1D-F). Next, we demonstrated the cytotoxicity of WT p53 in a dose-dependent manner through in vitro assays assessing the colony-forming ability compared to the controls (Supplementary Figure S1G). Similar experiments in additional HGSOC cell lines (OVCAR-3 and -5) corroborated growth inhibition, cell cycle arrest, induction of apoptosis, and reduction in colony-forming ability upon WT p53 expression (Supplementary Figure S2). Collectively, these data indicate that rescuing p53 function by vector-based re-expression of WT p53 induced cell cycle dysregulation and death in HGSOC cells and occurs in a dose-dependent manner.

3.2 | Design, generation, and characterization of IVT mRNAs in HGSOC cell lines

Recently, the therapeutic use of IVT mRNA as a vaccine has fueled great hope in the fight against infectious diseases. However, whether this class of biological agents is suitable for improving precision medicine targeting cancer remains elusive. To address this unanswered question, we used an IVT system based on a bacterial vector including a T7 RNA Polymerase promoter for the transcription of mRNAs (human p53, firefly luciferase [Luc], and EGFP), considering aspects of translational efficacy and decay rates of mRNA [26] (Supplementary Figure S3A). In vitro-transcribed mRNAs like IVT-Flag-tagged p53-mRNA, dubbed here as p53-mRNA, were analyzed using agarose gel electrophoresis for quality control (Supplementary Figure S3B).

Based on the clinical advantages of liposomes as carriers of chemotherapeutics over conventional chemotherapy due to reduced therapeutically side effects and increased anti-cancer activity [43, 44], we exploited a liposomal system using Lipofectamine Messenger MAX Transfection Reagent® by testing its supportive quality for the delivery of IVT-mRNA (EGFP-mRNA, Luc-mRNA) to the HGSOC cells. To quantitatively study the uptake of the control EGFP-mRNA, EGFP expression was measured using FACS as a surrogate marker for transfection efficiency. At 24 h following transfection with EGFP-mRNA (0.1–2 μ g), a dose-dependent increase in EGFP expression was detected (Supplementary Figure S3C). Although 0.25 μ g EGFP-mRNA was sufficient for expression in 90% of cells, at higher doses (0.5–2 μ g), 97%–100% of cells showed EGFP fluorescence, supporting an excellent transfection efficiency in the HGSOC cells (Supplementary Figure S3C). This observation was confirmed by WB, which showed high levels of EGFP at doses of ≥ 0.25 μ g EGFP-mRNA (Supplementary Figure S3C). In time kinetics, a high

percentage of EGFP-expressing cells (92.2%-99.7%) persisted for 10 days following transfection and declined to baseline levels ($\leq 5.5\%$) on day 15 (Supplementary Figure S3D). The EGFP expression was corroborated for a period of 7 days by WB (Supplementary Figure S3D). As a second control IVT-mRNA, Luc-mRNA transfection was monitored by WB, and activity measurements showed high enzymatic activity in cells transfected with 0.25-2 μg Luc mRNA (Supplementary Figure S3E).

To further validate the usefulness of our approach for the expression of a protein of choice driven by IVT mRNA in the HGSOC, we tested additional cell lines (OVCAR-3, -4, -5, and -8) and primary cells using immunofluorescence (Supplementary Figure S3F), FACS (Supplementary Figure S3G), and WB (Supplementary Figure S3H). Strong expression with 72% and 86% could be detected in OVCAR-5 and primary HGSOC cells, respectively, and very strong expression ($\geq 95\%$) in the OVCAR-3, -4 and -8 cells (Supplementary Figure S3G-H) transfected with 1 μg EGFP-mRNA. Collectively, different experiments demonstrated the high efficiency of liposomal-based IVT mRNA transfection and expression, irrespective of the OC cell line, primary cells, or type of mRNA.

3.3 | Characterization of mRNA expression in primary human cells and a mouse model

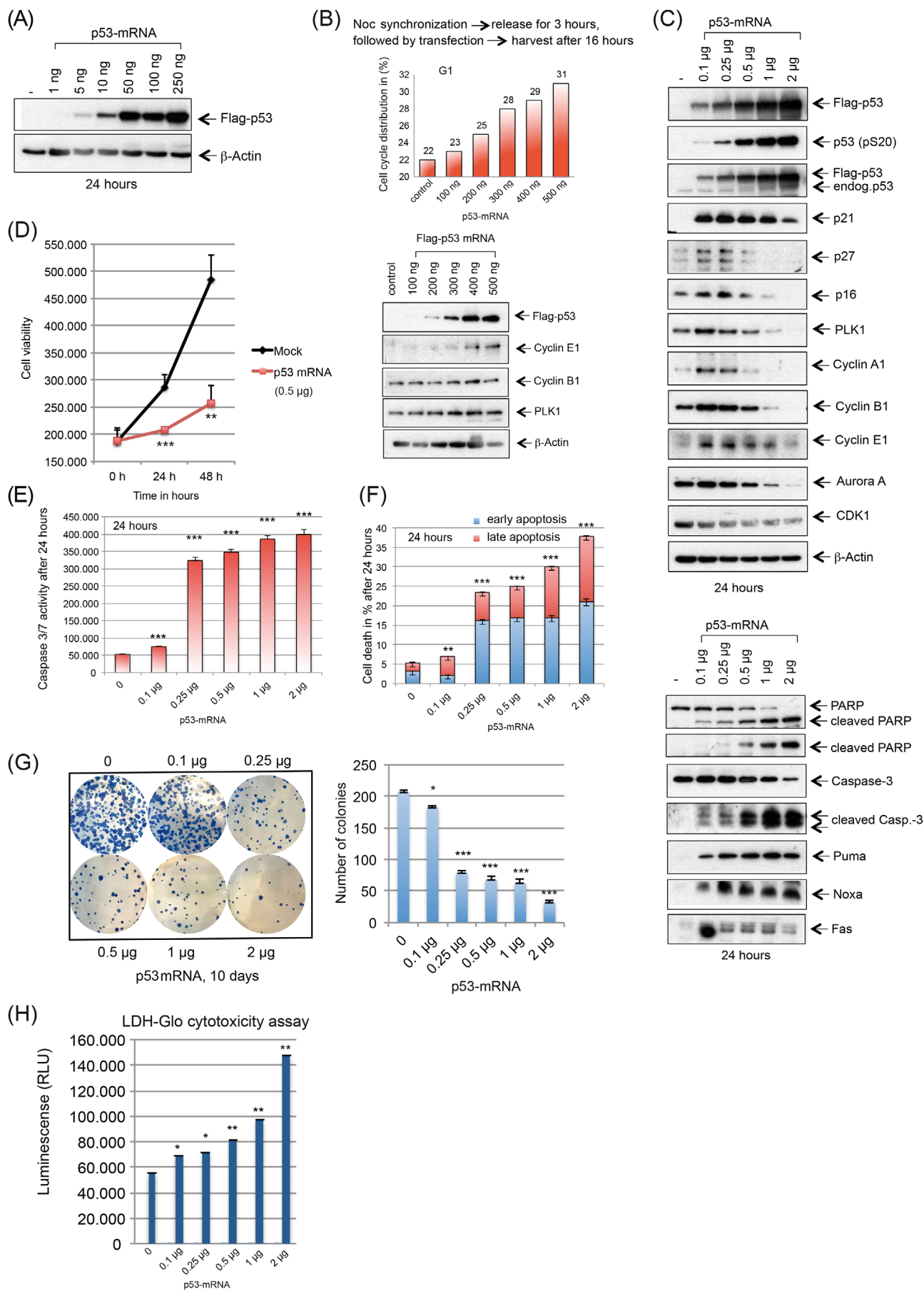
We investigated the time kinetics of EGFP and Luc mRNA expression in primary HGSOC cells. The EGFP expression using 1 μg mRNA could be detected in FACS studies on day one with 85% positive cells decreasing to 74% on day 11 and by WB for at least 7 days (Supplementary Figure S4A). Upon transfection of Luc-mRNA, enzymatic activity was detectable for 7 days, and WB signals were detectable for 4 days (Supplementary Figure S4B). Organoids from primary HGSOC showed efficient Luc activity or EGFP expression for up to 5 days (Supplementary Figure S4C-D). To monitor the duration of Luc activity in the mice by *in vivo* BLI, we transfected the OVCAR-8 cells with Luc mRNA (Supplementary Figure S4E) for subsequent application to the mice: (I) orthotopic implantation of 1×10^6 OVCAR-8 cells transfected with 2 μg Luc mRNA; (II) intraperitoneal injection of 2×10^6 OVCAR-8 cells transfected with 4 μg Luc mRNA, or (III) intraperitoneal injection of 10 μg liposomal Luc-mRNA (Supplementary Figure S4F). Luc activity was detectable for 2-3 days in all three experimental settings. Overall, the liposomal IVT mRNA was well suited to support efficient protein expression in primary human cells in cell culture and *In vivo* over several days.

3.4 | mRNA-based reactivation of p53 in HGSOC cells induces cell cycle arrest and cell death

We aimed to rescue p53 function in different preclinical models by transfecting HGSOC cell lines and primary cells with p53-mRNA. Low amounts of p53-mRNA (10-250 ng) strongly induced p53 protein expression in OVCAR-8 cells (Figure 1A). An increase in cells in G1 was observed at 100-500 ng p53-mRNA 24 h post-transfection compared to the controls (Figure 1B), supporting the reactivation of p53 activity. Strong induction of the cell cycle inhibitors, p21, p16, and p27, was readily visible at low doses of p53-mRNA ($\geq 0.1 \mu\text{g}$) in parallel with the downregulation of critical regulators, such as PLK1, Aurora A, CDK1, and Cyclin A/B, corroborating our results using a vector-based re-expression of p53 (Figure 1C). These observations correlated with a significant drop in cellular viability by ~ 2 -fold after 48 h at a dose of 0.5 μg (Figure 1D), accompanied by the rise of different indicators of cell death, such as Puma, Noxa, and Fas, cleaved PARP, cleaved Caspase-3 compared with untreated controls (Figure 1C), and increased caspase 3/7 activities (Figure 1E), and Annexin staining (Figure 1F). Loss of colony formation ability was induced by increasing the concentration of p53-mRNA (Figure 1G). We additionally performed a cytotoxicity assay, which confirmed previous observations of the impact of IVT P53 mRNA on ovarian cancer cells using apoptosis and colony forming assays (Figure 1H). Moreover, we tested p53-null HGSOC cells, such as OVCAR-5, for their sensitivity to re-expression of WT p53. Within 24 h following the p53-mRNA transfection, prominent signs of cell death, including strong PARP cleavage (Supplementary Figure S5A), high levels of cells in the sub-G1 phase (Supplementary Figure S5B), and high levels of caspase 3/7 (Supplementary Figure S5C) were observed. The performed cytotoxicity assays also confirmed previous observations of the impact of IVT P53 mRNA on OVCAR-5 cancer cells using the LDH-Glo cytotoxicity Assay (Supplementary Figure S5D). Overall, our observations indicated that rescuing p53 function by transfection of WT p53-mRNA induced cell death in different HGSOC cell lines.

3.5 | Reinstating p53 reduces numerical chromosomal instability (nCIN) in the HGSOC cell line OVCAR-8

Chromosomal instability is a fundamental feature of OC and most human OC cells exhibiting aneuploidy [45-47]. The OVCAR-8 cell line is classified as a hyperdiploid cell line with a high numerical complexity and modal number



of chromosomes ranging between 50-59 [45]. Thus, we aimed to determine whether restoring functional WT p53 could reduce the number of chromosomes in cells to a near-diploid status. Therefore, the cells were treated every two days for 28 days with low doses of p53-mRNA, and the distribution of chromosomes was assessed at the end of the incubation period (Figure 2A-B). The mean chromosome number was reduced from 53 to 47 upon restoration of WT p53 (Figure 2C-D).

The HGSOc subtype is characterized by increased replicative stress [48], resulting from various factors, including frequent loss of *TP53* [49]. This loss of *TP53* function contributes to replicative stress by compromising the DNA damage response mechanisms [49], which may partly explain the increased genetic instability observed in the OVCAR-8 cells. To quantify the extent of replicative stress in the OVCAR-8 cells before and after the restoration of p53 function, we assessed Ser139-phosphorylated H2AX foci (γ -H2AX) as a reliable marker of replicative stress and the presence of DNA double-strand breaks [50] after 7 and 14 days. We found that the baseline level of γ -H2AX foci decreased significantly over the treatment period from an average of 8 to 3 foci after 14 days in the OVCAR-8 and p53 mRNA-treated OVCAR-8 cells (Figure 2E). This result provided further evidence for the critical role played by p53 in maintaining genomic integrity in the HGSOc cells, most likely by counteracting replicative stress.

3.6 | mRNA-based rescue of p53 function in primary HGSOc cells induces cell cycle arrest and cell death

To further validate the rescue of p53 expression in a pre-clinical scenario, we compared the effects of p53-mRNA

transfection in primary normal ovarian and HGSOc cells. The expression of p53 was detected in all the primary samples, except the keratinocytes (Figure 3A). The first comparison of HGSOc and corresponding normal ovarian tissue from the same patient revealed higher expression of p53 in tumor cells, despite equal amounts of transfected p53-mRNA (Figure 3A). Analysis of additional patient-derived tissues confirmed that the expression of p53 and caspase 3/7 activity in all the tumor samples (Figure 3B) were significantly higher than the corresponding levels in the normal ovarian cells. In contrast, nearly the same levels of EGFP expression were observed in the normal and tumor cells upon transfection with equal amounts of IVT-EGFP mRNA (Supplementary Figure S6A). After testing the transfection efficacy of fluorescent mRNA in the normal and HGSOc patient-derived cells, no difference was detected (Supplementary Figure S6B), suggesting that different transfection efficiencies did not seem to be the reason for the different p53 levels compared to the primary cells (HGSOc vs. normal).

The WB examination revealed the upregulation of the inhibitors, p21 [51], p16, and p27 (Figure 3C) and apoptosis (Figure 3D), which was stronger in the p53-mRNA-transfected primary HGSOc cells compared to their normal counterparts, correlating with a more pronounced reduction in the number of HGSOc colonies (Figure 3E), which was corroborated by the LDH-Glo cytotoxicity assay (Figure 3F). Analysis of different HGSOc patients-derived organoids also demonstrated a significant decrease in volume and an increase in caspase 3/7 activity upon p53-mRNA-treatment under 3D cell culture conditions (Figure 3G). In summary, although the expression of p53 reduced the viability of both types of primary cells (normal vs. HGSOc), the effect was significantly stronger in the primary HGSOc cells compared to that in the normal cells,

FIGURE 1 Liposomal transfection of in vitro-transcribed WT p53-mRNA induces cell cycle arrest and apoptosis in the HGSOc cell line OVCAR-8. (A) OVCAR-8 cells were transfected with increasing amounts of liposomal IVT Flag-tagged WT p53-mRNA. Cell lysates were subjected to WB using Flag- and β -Actin-antibodies. (B) The dose-dependent cell cycle distribution of Nocodazole-synchronized cells is represented as a bar graph (upper panel; $n = 3$). Cell lysates were subjected to WB using Flag-, Cyclin E1-, Cyclin B1-, PLK1-, and β -Actin-antibodies (lower panel). (C) Cell lysates were subjected to WB for key mediators of cell cycle regulation using Flag-, p53 (pS20)-, p53-, p21-, p27-, p16-, PLK1-, Cyclin A1-, Cyclin B1-, Cyclin E1-, Aurora A-, CDK1-, and β -Actin-antibodies (upper panel). The same cell lysates were subjected to WB for regulators of apoptosis using PARP-, Caspase-3-, Puma-, Noxa-, and Fas-antibodies (lower panel). (D) Cells were mock- or 0.5 μ g p53-mRNA-transfected, and proliferation was measured using a CellTiter-Blue Cell Viability assay, 24 h post-treatment. $**P < 0.01$, $***P < 0.001$, Student's t-test, unpaired and two-tailed. (E) The dose-dependent Caspase-3/7 activities were determined using a Caspase-Glo 3/7 assay. $***P < 0.001$, Student's t-test, unpaired and two-tailed. (F) Graphical representation of Annexin V positive (%) cells. FACS analysis of transfected cells, gated for Annexin V positive (early apoptotic), and Annexin V/7AAD positive (late apoptosis) populations is demonstrated. $n = 3$ for each dose; $**P < 0.01$, $***P < 0.001$. (G) Representative images show the number of 3D colonies (dose-dependent) on day 10 (left panel). The dose-dependent distribution of colonies is represented as bar graph (right panel; $n = 3$). $*P < 0.05$, $***P < 0.001$, Student's t-test, unpaired and two-tailed. (H) Graphical representation of the cell cytotoxicity caused by increasing concentrations of transfected p53 mRNA. $n = 3$ for each concentration; $*P < 0.05$, $**P < 0.01$. Aurora-A, Aurora Kinase A; CDK1, cyclin-dependent kinase 1; FACS, Fluorescence-Activated Cell Sorting; Fas, Tumor necrosis factor receptor superfamily member 6; HGSOc, High-Grade Serous Ovarian Cancer; IVT, in vitro-transcribed; Noxa, NADPH oxidase activator 1; p53, tumor protein p53; PARP, Poly (ADP-ribose) polymerase; PLK1, Polo-like kinase 1; WB, western blot.

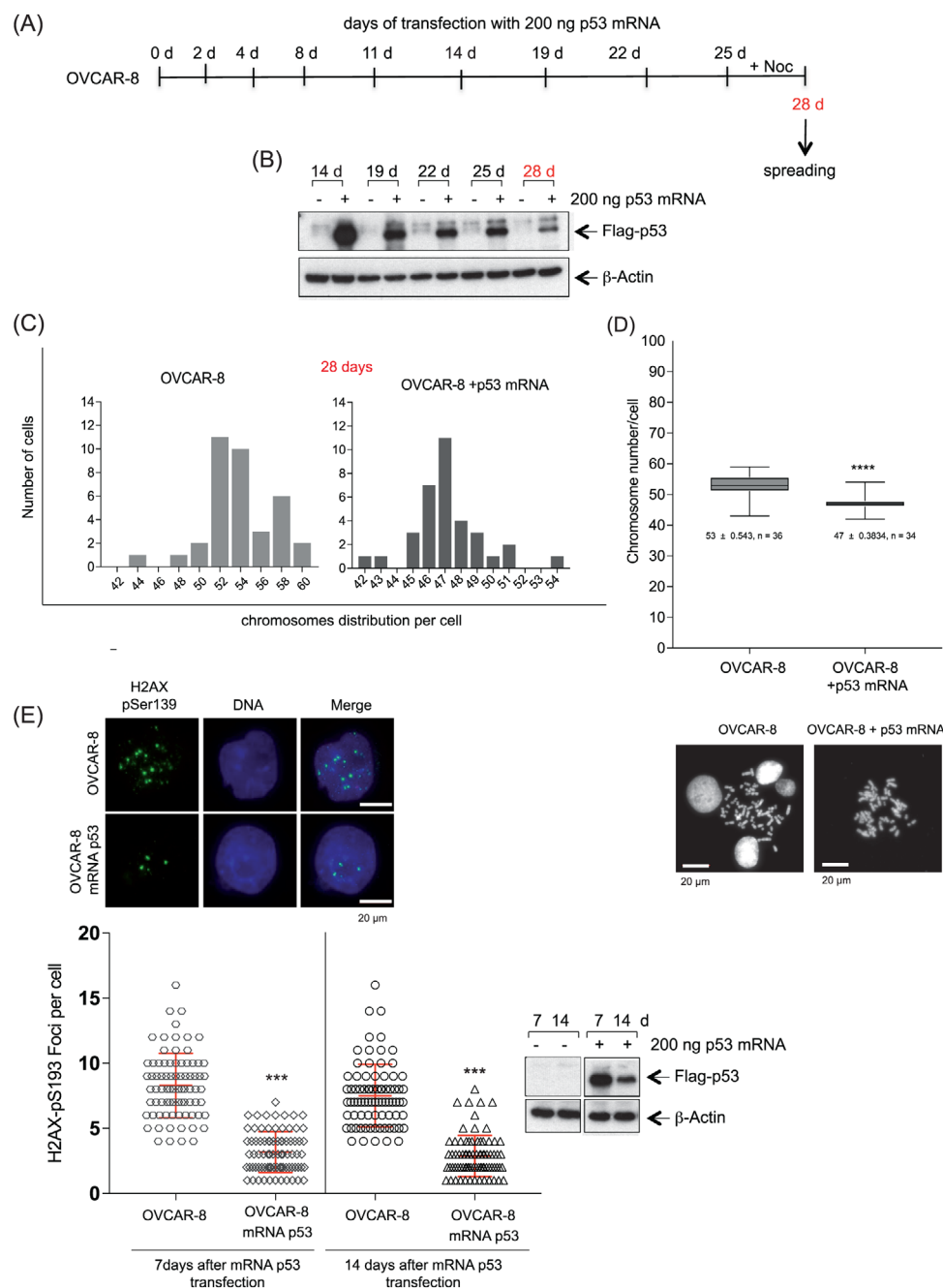
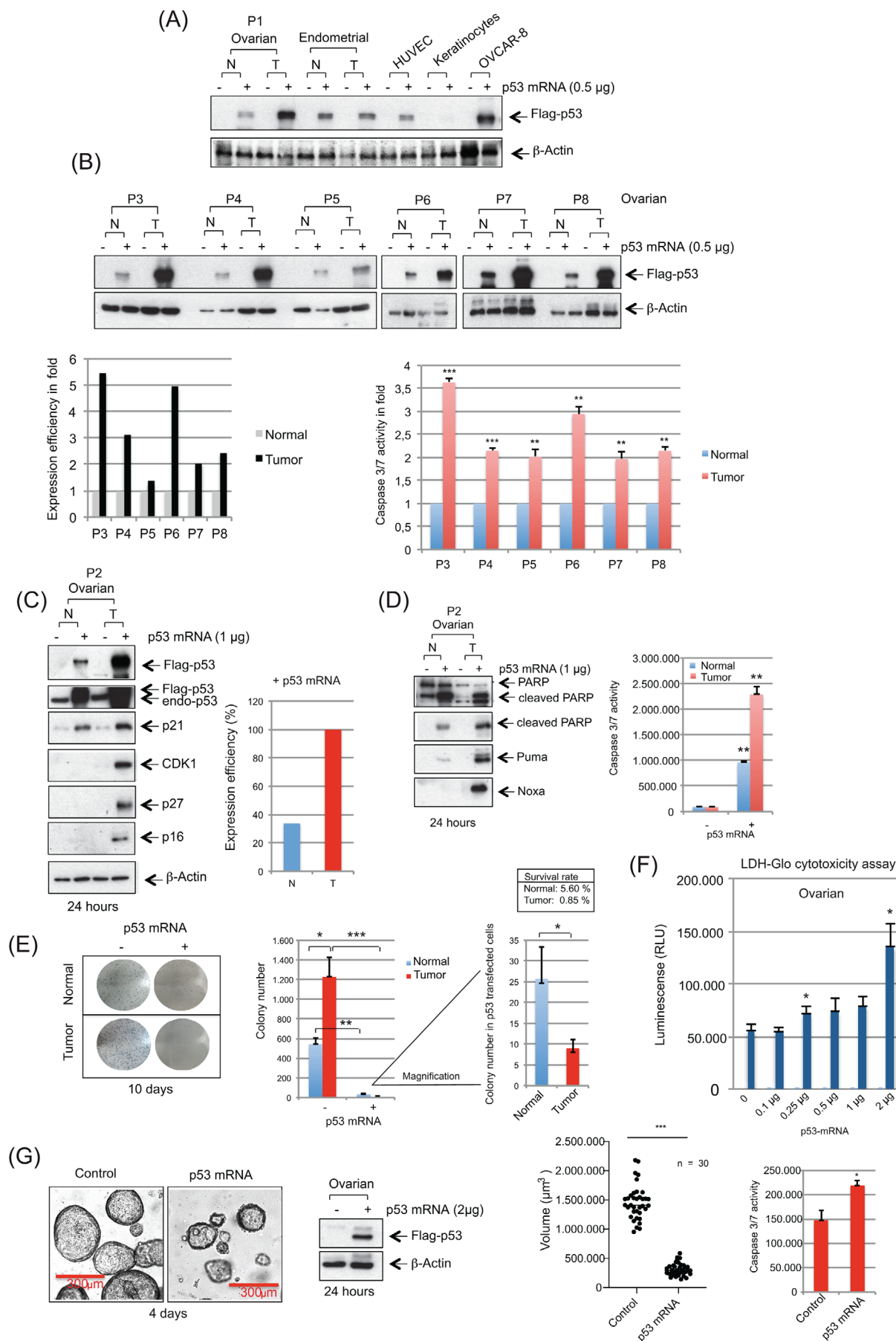


FIGURE 2 Restoring p53 function reduces nCIN in OVCAR-8 cells. (A) Treatment schedule. OVCAR-8 cells were kept in culture for 28 d and treated with 200 ng p53-mRNA every 48 h. Metaphase spreading of untreated controls and treated OVCAR-8 cells were prepared at the end of the incubation. Chromosomes were stained with Hoechst. (B) Western blot of p53-mRNA expressing OVCAR-8 using Flag- and β -Actin-antibodies. (C) Histogram plots of the distribution of chromosome numbers in controls and cells treated with 200 ng p53-mRNA. (D) Quantification of the number of chromosomes in cells with/without p53-mRNA-treatment (upper panel). The results were analyzed statistically, mean \pm SD, **** $P < 0.001$. Representative images of metaphase chromosome spreads (lower panel). Green, H2AX pSer193; blue, DAPI. Scale bar = 20 μ m. (E) IF images showing OVCAR-8 and OVCAR-8 + mRNA p53 cells with H2AX pSer193 foci staining 15 days post-treatment with mRNA p53 (upper left panel). Scale bar = 20 μ m. Quantification of H2AX pSer193 foci 14 days post-treatment with mRNA p53 (lower left panel). The results are presented as mean \pm SEM, $n = 85$ cells, *** $P \leq 0.001$. OVCAR-8 cells were kept in culture for 14 days and treated with 200 ng p53-mRNA every 48 h (lower right panel). Cell lysates were subjected to WB using Flag- and β -Actin-antibodies. d, day; H2AX pSer193, H2A histone family member X phosphorylated at Ser193; nCIN, numerical chromosomal instability; p53, tumor protein p53; SD, standard deviation; IF, Immunofluorescence; SEM, standard error of the mean.



which could be due to elevated levels of p53 in the tumor cells.

3.7 | Transcriptome alterations in OVCAR-8 cells upon rescue of WT p53 functions

Our observations of reduced proliferative activity and increased cell death in the cell lines and primary cells of HGSOC origin support the model of rescued p53 function upon p53 re-expression by mRNA transfection. To deepen our understanding of the underlying biological processes and address this aspect in a relatively unbiased manner, we transfected the OVCAR-8 cells with 1 μ g p53-mRNA or mock control (EGFP mRNA) in three independent experiments. In total, 25,540 human genes were profiled by RNA-seq 24 h after the transfection (Supplementary Figure S7A-B). Both groups were compared using unpaired *t*-tests, considering group variance. Transcriptomic analysis revealed that 3,061 transcripts were upregulated, and 1,662 were downregulated (Figure 4A-B). These significant genes were further analyzed with the IPA software to identify overrepresented canonical pathways associated with the p53-mRNA transfection (Figure 4C, Supplementary Figure S7C).

Consistent with the pro-apoptotic functions of p53 as a tumor suppressor involved in the induction of cell cycle arrest and apoptosis, our IPA revealed an overrepresentation of several related pathways upon p53-mRNA transfection, such as “p53 signaling”, “apoptosis signaling”, and several “cell cycle” pathways (Figure 4C). To confirm these findings, we investigated all genes involved in the IPA “p53 signaling” pathway and we realized that

most of them (51/81, 63%) were differentially expressed with FDR $q < 0.05$ and absolute FC > 1.5 (Figure 4D). Notably, most known downstream targets of p53 signaling (96%) were coordinately upregulated by mRNA transfection of p53-mRNA (Figure 4D). We further validated these results by performing WB of selected proteins from the p53 signaling pathway, including p21 (*CDKN1A*), MDM2, Puma (*BBC3*), p73, FAS (*CD95*), and CDK1 (Figure 4E). Their expression in the OVCAR-8 cells was substantially upregulated or downregulated by p53-mRNA in agreement with transcriptomic analysis. Most genes in the apoptosis signaling pathway (44/68, 65%) were significantly deregulated (Supplementary Figure S8A). We extensively validated 12 of these proteins using WB (Supplementary Figure S8B) to demonstrate that p53-mRNA transfection induces apoptosis in the OVCAR-8 cells.

Several “cell cycle” pathways, including “cell cycle control of chromosomal replication”, “cell cycle: G2/M DNA damage checkpoint regulation”, and “cyclins and cell cycle regulation”, were significantly overrepresented, as well as “Mitotic roles of Polo-like kinase” [52, 53], and they showed a global downregulation (negative *z* score) (Figure 4C). Most of the genes from these pathways were differentially expressed (Supplementary Figure S9A-B) and validated using WB (Supplementary Figure S9C), confirming the downregulation of the cell cycle and mitotic roles of PLK1. Remarkably, the cellular senescence pathway was also upregulated and may contribute to cell death along with the induction of apoptosis (Figure 4C).

Next, we carried out a transcriptome comparison between the primary HGSOC cells from patient one and the OVCAR-8 cells, of which both were p53-mRNA-transfected (Figure 5A). The high variability among the

FIGURE 3 Liposomal transfection of p53-mRNA results in higher p53 expression in primary HGSOC cells compared to their normal counterparts. (A) Primary human cells of different origins (tumor, normal) and OVCAR-8 cells were transfected with p53-mRNA. Cell lysates were subjected to WB using Flag- and β -Actin-antibodies. (B) Primary human HGSOC cells (tumor, normal) derived from patients P3-8 were transfected with 0.5 μ g p53-mRNA. Cell lysates were subjected to WB using Flag- and β -Actin-antibodies (upper panel). (lower left) Expression efficacy was depicted as bar graphs (lower left panel). Caspase 3/7 activities were determined using a Caspase-Glo 3/7 assay (lower right panel). $**P < 0.01$, $***P < 0.001$. Student's *t*-test, unpaired and two-tailed. (C) Lysates of mock- or p53-mRNA-transfected normal ovarian or tumor HGSOC (patient 2) cells were subjected to WB using Flag-, p53-, p21-, CDK1-, p27-, p16-, and β -Actin-antibodies (left panel). The normalized levels of p53 expression are represented as a bar graph (right panel). (D) The same cell lysates were subjected to WB using PARP-, Puma-, and Noxa-antibodies (left panel). Caspase-3/7 activities of mock- or p53-mRNA-transfected normal and tumor HGSOC cells were determined using a Caspase-Glo 3/7 assay (right panel; $n = 3$). (E) Representative images show the 3D colonies of mock-transfected cells on day 10 (left panel). Representative images show the 3D colonies of p53 mRNA-transfected cells on day 10 (right panel; $n = 3$). $*P < 0.05$, $**P < 0.01$, $***P < 0.001$. Wilcoxon test, unpaired and two-tailed. (F) Graphical representation of the cell cytotoxicity caused by increasing concentrations of transfected p53 mRNA. $n = 3$ for each concentration; $*P < 0.05$. (G) Representative images show organoids on day 4 after transfection with 2 μ g p53 mRNA (left panel). Lysates of HGSOC organoids (patient 3) mock- or p53-mRNA-transfected cells were subjected to WB using Flag- and β -actin-antibodies (middle left panel). Organoid size was determined using ImageJ (middle right panel; $n = 30$). $***P < 0.001$; Student's *t*-test, unpaired and two-tailed. Caspase-3/7 activities of HGSOC organoids mock- or p53-mRNA-transfected were determined using the Caspase-Glo 3/7 assay (right panel; $n = 3$). $*P < 0.05$; Student's *t*-test, unpaired and two-tailed. CDK1, cyclin-dependent kinase 1; HUVEC, human umbilical vein endothelial cells; N, normal tissue; Noxa, NADPH oxidase activator 1: P (1-8), patient-derived material ($n = 8$ patients); p53, tumor protein p53; PARP, Poly (ADP-ribose) polymerase; Puma, p53 upregulated modulator of apoptosis; T, tumor tissue.

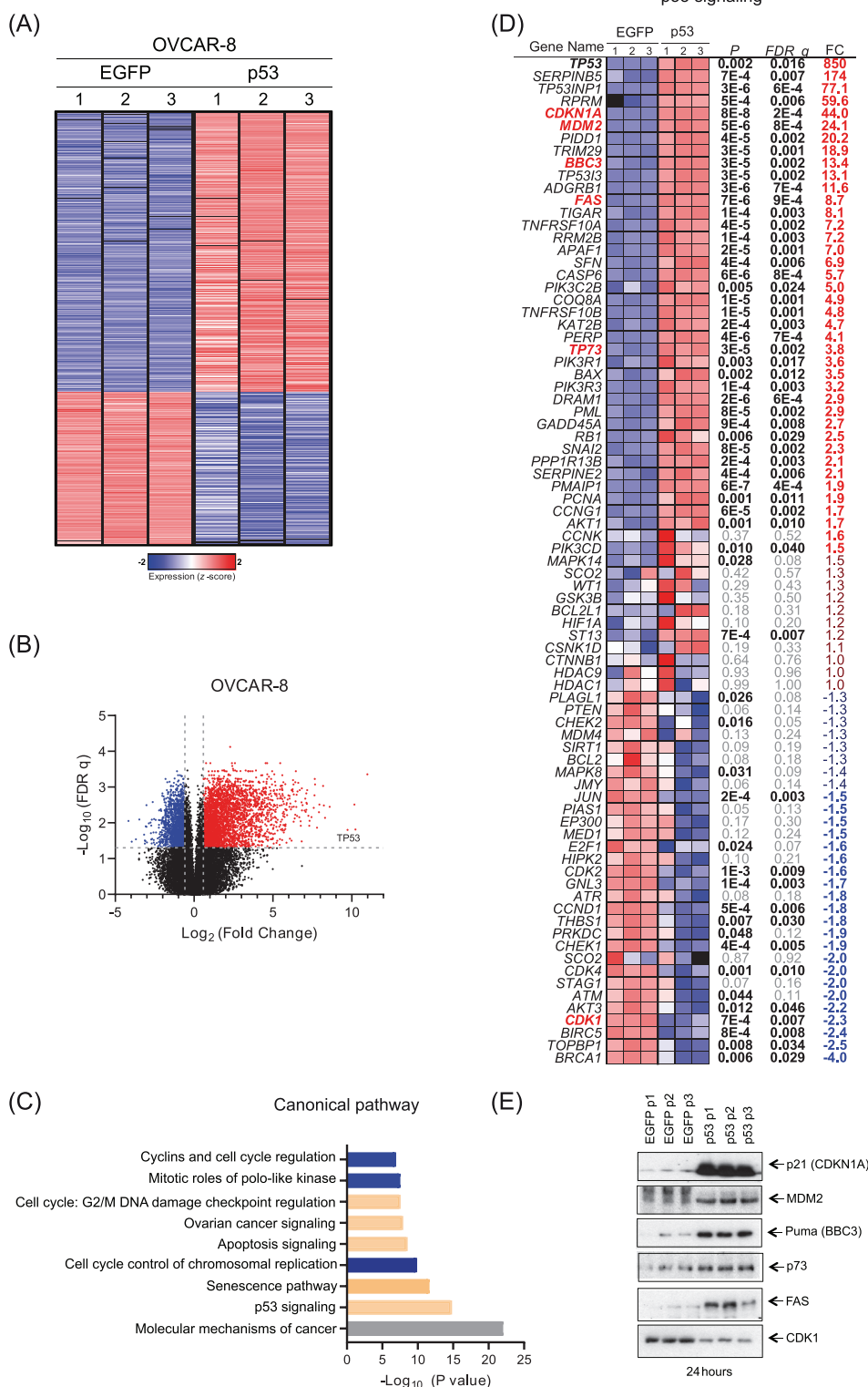


FIGURE 4 Identification of differentially expressed genes in p53-mRNA-transfected OVCAR-8 cells compared to mock-transfected counterparts. (A) Heatmap of normalized gene expression represented by z scores of OVCAR-8 cells treated with mock (EGFP mRNA) or p53-mRNA from three independent RNA-seq experiments (Student's *t* tests or Welch tests, depending on the variance, corrected by FDR *q* adjusted *P*-value < 0.05 and absolute FC > 1.5). (B) Volcano plot showing the DEGs in the RNA-seq between OVCAR-8 cells treated with EGFP vs. p53-mRNA (red dots = upregulated genes, blue dots = down-regulated genes). (C) Selected overrepresented Ingenuity pathways from pathway enrichment analysis of DEGs with FDR-adjusted *P*-values < 0.05 and FC > 1.5. Pathways with a positive z score, representing a global upregulation of the pathway genes, are depicted in orange; pathways with a negative z score, indicating a global gene downregulation

primary samples resulted in low significance after FDR correction for multiple testing. Thus, we considered the significance of the transcripts of primary HGSOC cells with $P < 0.01$ and $FC > 1.5$. A total of 156 transcripts were upregulated, and 115 were downregulated (Figure 5B-C). Several genes from the primary HGSOC cells were significant and similar to the pathways identified in the OVCAR-8 cells (Figure 5D), supporting the relevance of both datasets.

Consistent with the paramount function of p53 in OC development, our IPA showed multiple transcriptional alterations in the “ovarian cancer signaling” pathway. Many genes in this pathway (55/76, 72%), including Wnt/ β -catenin signaling, were significantly deregulated (Figure 6A-B). The Wnt/ β -catenin pathway promotes chemoresistance, metastasis, and cancer stem cell self-renewal in OC by the aberrant activation of Wnt/ β -catenin signaling, leading to-catenin hyperactivity [54]. Treatment with p53-mRNA resulted in upregulation of AXIN1, which functions as a scaffolding protein for components of the β -catenin destruction complex, including APC, CK1PP2A, and GSK3 β . Additionally, deregulation was observed in members of the frizzled receptor, Wnt, and TCF/LEF families (Figure 6A-B). Overall, these transcriptional alterations led to a moderate reduction of β -catenin (Figure 6B) and to the descending activity of Wnt signaling using a TCF/LEF reporter assay in the p53-mRNA-treated cells (Figure 6C).

3.8 | Orthotopical application of p53-mRNA-treated OVCAR-8 cells resulted in a dose-dependent reduction of tumor growth in an HGSOC Xenograft model

To explore the viability of the p53-mRNA-treated OC cells in a physiological microenvironment, an orthotopic disease model was used. First, we tested whether stable Luc-expressing OVCAR-8 cells (OVCAR-8/Luc) showed an altered response to p53-reactivation. Treatment with 100 ng p53-mRNA induced only moderate cell death, as evidenced by the low expression of apoptotic markers/activation, low caspase 3/7 activity, and moderate inhibition of cell growth, whereas transfection with 500 ng

p53-mRNA induced a robust apoptotic response and strong drop in colony-forming efficacy (Supplementary Figure S10A-C). Thus, the stable expression of Luc in OVCAR-8 cells did not alter the response to mRNA-dependent reactivation of p53 compared to that in WT cells.

One day prior to the xenograft experiment, the OVCAR-8/Luc cells were transfected with mock- or p53-mRNA (100 ng or 500 ng) (Figure 7A). To establish an orthotopic model, a Matrigel/OVCAR-8/Luc cell suspension was injected into the right ovary of each mouse. The determination of tumor volumes at 1 \times per week for an observation period of 10 weeks by BLI demonstrated growth retardation in tumors originating from cells treated with 100 ng p53-mRNA and a complete block of cellular proliferation upon treatment with 500 ng p53-mRNA (Figure 7B). To verify the luciferase activity in vivo, the mice were sacrificed at the end of the study and subjected to anatomical/histological examination of all organs by two independent veterinary histologists. The inspection of removed ovaries based on the determination of volume (Figure 7C) and BLI measurements (Figure 7D) confirmed the dose-dependent size reduction of the ovary tumors by p53 mRNA treatment supporting the In vivo BLI measurements (Figure 7B). Histological examination revealed huge tumor masses and profoundly altered morphology due to the vast carcinoma tissue in the right ovaries injected with mock-treated OVCAR-8/Luc cells. In the 100 ng p53-mRNA-treated group, the right ovaries exhibited low to medium amounts of tumors (Figure 7E, d-e) or normal histology. The right ovaries of the 500 ng p53-mRNA-treated group and all other organs showed normal histology (Figure 7E, g-h, Supplementary Figure S10D). In all treatment groups (mock, 100 ng, and 500 ng p53-mRNA), the left ovaries that did not receive OVCAR-8/Luc cells showed normal histology with follicular and luteal structures, as well as stromal tissue (Figure 7E, c-f-i). In the mice injected with mock-treated cells, metastases were detected in the intestine; metastatic activity in the 100-ng group was low and absent in the 500-ng group (Figure 7D-F). Overall, these animal data revealed dose-dependent growth retardation and blocked dissemination of p53-mRNA-treated OVCAR-8/Luc cells under orthotopic conditions.

in the pathway, are depicted in blue; and pathways with no specific pattern are depicted in gray. (D) Heatmap of all genes corresponding to the “p53 signaling pathway” from IPA, indicating the P -value, FDR-adjusted P -value and FC for the comparison of EGFP with p53-mRNA. Genes with validation by WB are highlighted in red. (E) Cell lysates were subjected to WB for p53 signaling pathways using p21, MDM2, Puma, p73, Fas, and CDK1 antibodies. CDK1, cyclin-dependent kinase 1; DEG, differentially-expressed gene; EGFP, enhanced green fluorescent protein; Fas, tumor necrosis factor receptor superfamily member 6; FC, fold change; FDR, false-discovery rate; IPA, Ingenuity Pathway Analysis; MDM2, double minute 2 homolog protein; Puma, p53 upregulated modulator of apoptosis; Noxa, NADPH oxidase activator 1; p53, tumor protein p53; RNA-seq, RNA sequencing.

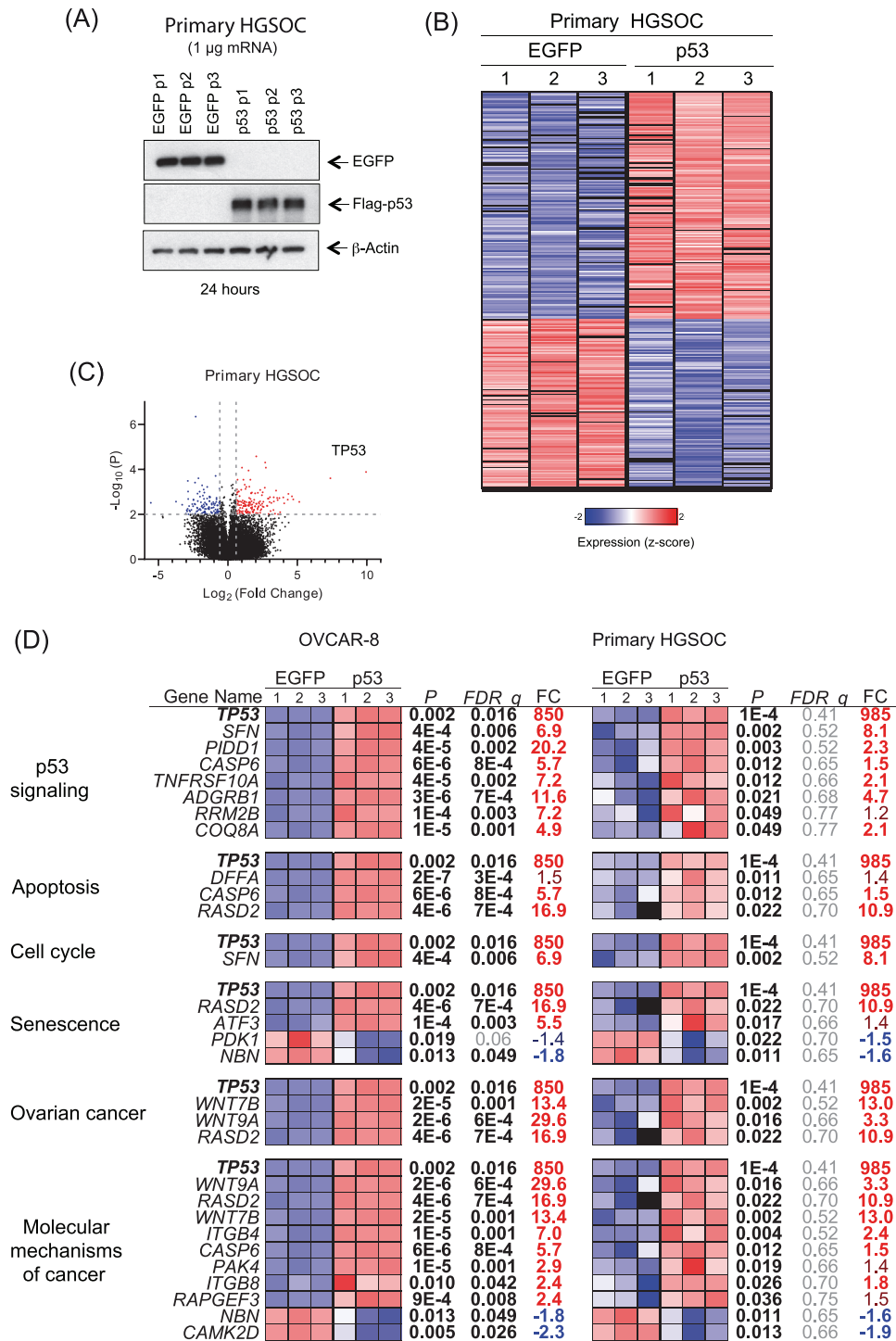


FIGURE 5 Analysis of differentially expressed genes in primary HGSOC cells. (A) Primary HGSOC cells from patient 1 were transfected with p53-mRNA or EGFP-mRNA. Cell lysates were subjected to WB using EGFP, Flag, and β -Actin antibodies. (B-C) Heatmap (B) and volcano plot (C) showing the DEGs in the RNA-seq between primary HGSOC cells treated with EGFP vs. p53-mRNA (P value < 0.01 and absolute FC > 1.5 ; red dots = upregulated genes, blue dots = down-regulated genes). (D) Transcriptome analysis of DEGs in common with OVCAR-8 and primary HGSOC cells for selected significant overrepresented Ingenuity pathways. EGFP, enhanced green fluorescent protein; FC, fold change; DEG, differentially-expressed gene; HGSOC, high-grade serous ovarian cancer; RNA-seq, RNA sequencing; TP53, tumor protein p53.

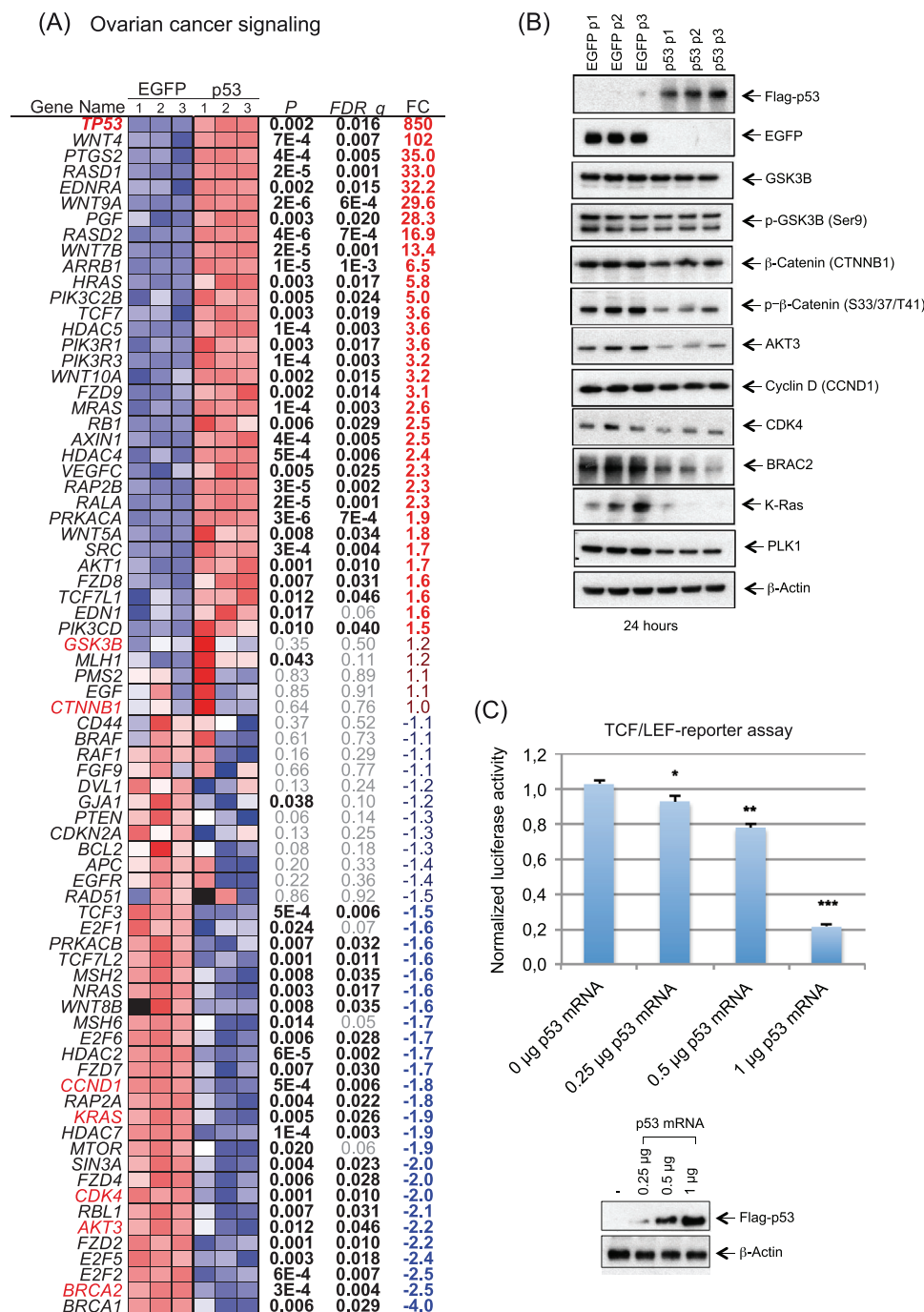
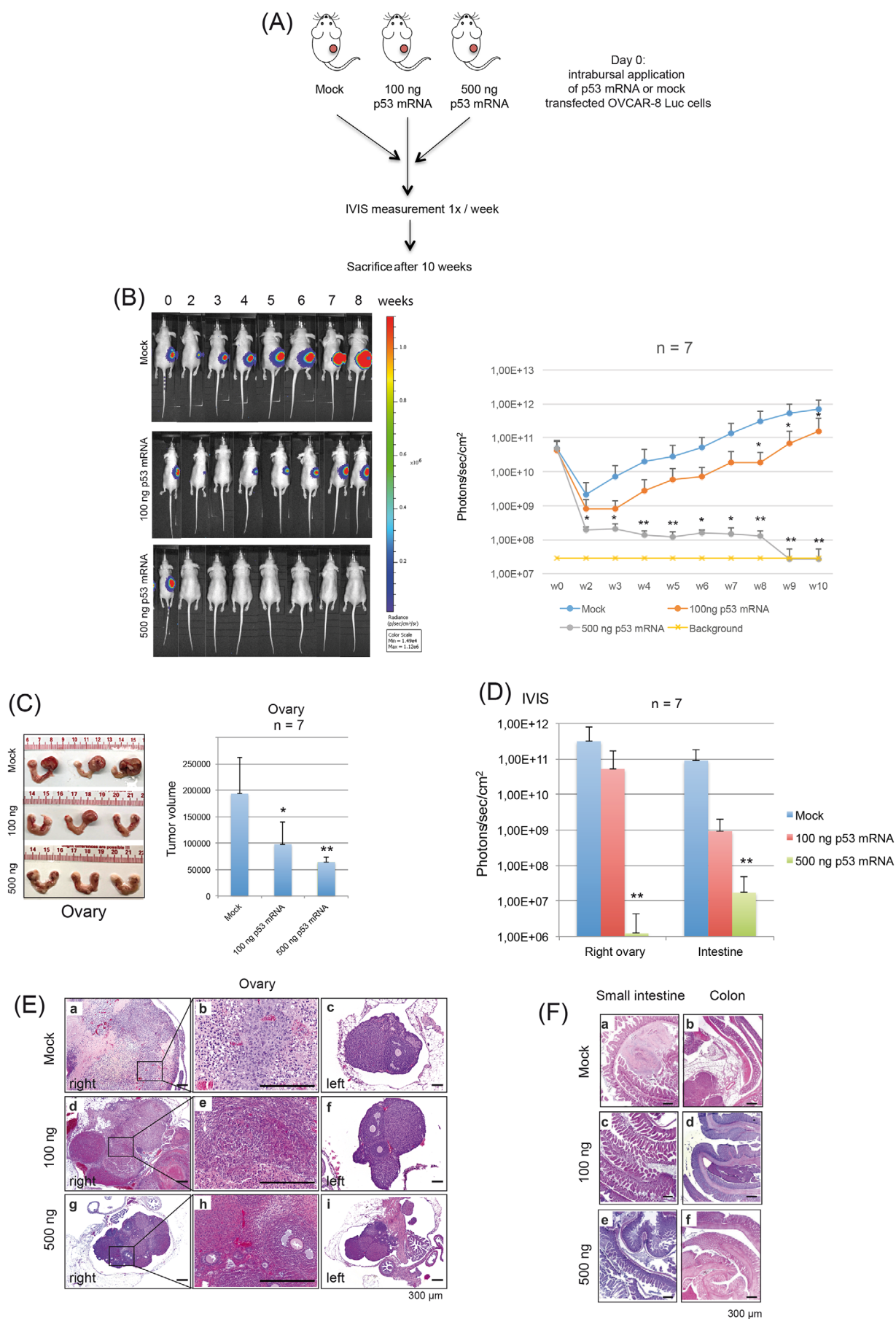


FIGURE 6 OC signaling pathway upregulation upon treatment of OVCAR-8 cells with IVT p53-mRNA. (A) Heatmap of all genes corresponding to the OC Signaling pathway from IPA, indicating the *P* value, FDR-adjusted *P* value, and FC for the comparison of EGFP with p53-mRNA in OVCAR-8 cells. (B) WB analysis using Flag-, EGFP-, GSK3B-, p-GSK3B-, β-Catenin-, p-β-Catenin-, AKT3-, Cyclin D-, CDK4-, BRCA2-, K-Ras-, PLK1-, and β-Actin-antibodies. (C) TCF/LEF luciferase reporter responses of cells transfected with increasing doses of p53-mRNA. WB analysis using Flag- and β-Actin-antibodies. (ser9), phosphorylated Glycogen synthase kinase 3β AKT3, V-Akt murine thymoma viral oncogene homolog 3; at serine 9; BRCA2, breast cancer gene 2; CDK4, cyclin-dependent kinase 4; CTNNB1, β-Catenin; EGFP, enhanced green fluorescence protein; FC, fold change; GSK3β, glycogen synthase kinase 3β; p-GSK3β IPA, Ingenuity Pathway Analysis; WB, western blot; IVT, in vitro transcribed; K-ras, kristen murine sarcoma virus 2 homolog; OC, ovarian cancer; p53, tumor protein p53; PLK1, Polo-like kinase 1.



3.9 | Intraperitoneal application of OVCAR-8 cells followed by intraperitoneal treatment with p53-mRNA inhibited dissemination of tumor cells

To further validate the clinical relevance of p53-mRNA in metastatic HGSOc, we tested whether the scattered tumor cells within the peritoneum were accessible to liposomal p53-mRNA. The intraperitoneal administration of drugs for OC was shown to be more efficacious than systemic administration and was recommended by the National Cancer Institute [55]. Along these lines, we injected 2×10^6 OVCAR-8/Luc cells intraperitoneally and administered p53-mRNA 4–6 h later via the intraperitoneal route. The mice were treated for three weeks with 2 intraperitoneal injections per week with p53-mRNA (0.16 mg/kg) or control. Although the OVCAR-8/Luc cells treated with the control grew exponentially, the intraperitoneal treatment with the liposomal p53-mRNA completely blocked the tumor cell growth (Figure 8A). During the entire observation period, the body weights of the mice in both groups developed normally (Figure 8B).

In the control mice receiving intraperitoneal OVCAR-8/Luc cells and intraperitoneal mock treatment, gross anatomical analysis revealed tumor masses on the peritoneal surfaces (Figure 8C–D). Most of these metastases were weakly attached to the organs. Large tumors were also detected in fatty tissues, such as the omentum, ovarian fat pad, and mesentery (Figure 8C–D). In particular, larger tumor masses attached to the small and large intestines lead to adhesion between intestinal structures, implicating strictures of the gut. The IVIS measurements of the omentum and intestine revealed the most prominent signals, correlating with the histological results (Figure 8D–E). In the mice treated with p53-mRNA, gross anatomical and histological analyses did not reveal tumor masses in the

peritoneal cavity, and all the organs appeared normal upon visual inspection. The IVIS measurements and histological inspection did not provide evidence of tumor cell dissemination (Figure 8D–E).

4 | DISCUSSION

In this study, we sought to restore p53 functionality in HGSOc using IVT p53 mRNA. Re-expression of WT p53 resulted in a significant reduction in cell proliferation, induction of apoptosis, and perturbations in cell cycle dynamics in the HGSOc cells. The liposomal delivery system demonstrated high transfection efficiency and sustained mRNA expression. Furthermore, the p53 IVT-mRNA transfection in primary HGSOc cells yielded similar outcomes, including cell cycle arrest, apoptosis induction, and diminished cell viability, compared to normal ovarian cells. Transcriptome analysis revealed notable alterations in pathways related to p53 signaling, apoptosis, and cell cycle regulation. In an in vivo setting, p53 IVT mRNA treatment effectively inhibited tumor growth and prevented tumor cell dissemination within the peritoneal cavity. These findings underscore the potential utility of mRNA-based strategies for reactivating p53 and combating HGSOc by inducing programmed cell death, orchestrating cell cycle checkpoints, and reducing tumor progression and metastasis.

Mutations in p53 occur in up to 96% of patients with HGSOc [13]. Researchers have attempted to reactivate p53 and suppress OC growth using WT p53 gene therapy [56]. However, therapies using WT Ad-p53 (Gendicine, Advexin, SCH-58500), liposomal WT p53, or p53-specific conditionally replicative adenoviral vectors have not yet been approved as p53-based drugs for HGSOc therapy. Recent studies have demonstrated that novel IVT-mRNA-

FIGURE 7 Application of liposomal p53-mRNA to OVCAR-8 cells prevents intrabursal growth and dissemination in an orthotopic mouse model. (A) Schematic design of the orthotopic murine model. (B) Bioluminescence imaging. One day before, Luc-expressing OVCAR-8 cells were transfected (mock, 100 ng p53-mRNA, or 500 ng p53-mRNA) (left panel). Approximately 1×10^6 cells per mouse were injected into the bursa (right ovary) of nude mice on day 0 and imaged using the IVIS Lumina system following D-luciferin application. Eight weeks following orthotopic application of OVCAR-8 cells (mock- or p53-mRNA-treated) representative images of the mice (one per week) at baseline are shown. Photon flux is indicated in the pseudocolored heat map. BLI was performed at the indicated time points and data were presented in a graphic (right panel). Photon flux was normalized to baseline values obtained from the mice on day 0. * $P < 0.05$, ** $P < 0.01$. Wilcoxon test, unpaired and two-tailed. (C) Representative photographs of removed ovaries 10 weeks after intrabursal application of mock- or p53-mRNA-transfected (100 ng, 500 ng) OVCAR-8 cells in mice (left panel, $n = 7$ for each group). Analysis of extracted ovaries. The dose-dependent tumor volumes are represented as bar graph (right panel). * $P < 0.05$, ** $P < 0.01$. Wilcoxon test, unpaired and two-tailed. (D) BLI of removed, tumor-bearing organs 10 weeks after intrabursal application of mock- ($n = 7$), or p53-mRNA-transfected (100 ng, 500 ng) OVCAR-8 cells ($n = 7$ mice for each group) represented as bar graph. ** $P < 0.01$. Wilcoxon test, unpaired and two-tailed. (E) Hematoxylin and eosin-stained sections of ovaries injected with p53-mRNA-transfected (100 ng, 500 ng) ($n = 7$) or mock- ($n = 7$) OVCAR-8 cells at the end of the experiment (10 weeks). Scale bars, 300 μm . (F) Representative hematoxylin and eosin-stained sections of metastases at the small intestine and colon following intrabursal injection of mock-, or p53-mRNA-transfected (100 ng, 500 ng) OVCAR-8 cells (after 10 weeks). Scale bars, 300 μm . BLI, Bio-layer Interferometry; IVIS, In vivo imaging system; p53, tumor protein p53.



based therapeutics are powerful tools for developing novel vaccines [57]. Here, we explored the potential role of IVT mRNA for the reactivation of tumor suppressor functions in cancer. We first examined the functional aspects of mRNA expression in HGSOC cells using different IVT mRNA species (EGFP, luciferase, and Flag-p53). The translation of eukaryotic mRNA is a precisely controlled procedure in which the 5' Cap, 3', and 5' untranslated regions (UTRs) contribute significantly to the stability of the mRNA [26]. To reach this aim, we used here mRNA co-transcriptionally capped with m7G(5')ppp(5') (2'OMeA)pG. The 5' UTR contains an eIF4G aptamer that was previously shown to improve the translation efficacy of IVT mRNA. Additionally, in all the three mRNA used here, the four canonical bases (ACGU) were replaced by ACGPseudo-U, which was found to improve the functionality of IVT mRNA [58].

Our IVT-EGFP-mRNA with optimized structural features achieved 72%-99% expression in the HGSOC cell lines and up to 83% expression in the primary cells using liposomal transfection. High EGFP expression ($\geq 90\%$) lasted over 10 days in the cell lines and 4-11 days in 2D-cultured primary cells and in tumor organoids for 5 days, suggesting that liposomal IVT-mRNA transfection enables efficient, long-lasting expression in HGSOC cells. Interestingly, comparison of the primary HGSOC samples with their normal counterparts, both transfected with equal doses, showed much higher p53 expression in the tumor cells, resulting in more robust anti-proliferative effects in tumor cells. The p53 was previously found to be present at low levels in resting cells, but multiple cancer-related stress stimuli, such as hyper-induction of the HSP90 system, provoke post-translational modifications of p53 to modulate its protein stability [59]. Moreover, mutant p53 has been reported to be involved in the metabolic adaptation of cancer cells by sustaining the Warburg effect. By increasing glucose intake in tumor cells, mutant p53 hinders autophagy-dependent degradation caused by glucose deprivation [60]. Thus, the reprogramming of cancer cells increases the stability of mutant p53 through dif-

ferent mechanisms. Exogenous WT p53 expressed upon mRNA transfection may utilize these mechanisms for stabilization.

Our findings support the idea that restoring WT p53 function induces cell cycle arrest, apoptosis, and tumor suppression [61]. Sequencing of RNA revealed coordinated upregulation of multiple p53 target genes promoting cell death, including *p21*, *MDM2*, *PUMA*, *GADD45B*, *FAS*, *BAX*, and *FBXW7*, and downregulation of centromere-related components such as *BUB1*, *BUB1B*, *CDC20*, *APC*, and *PLK1*, along with crucial regulators of cell cycle progression (*CDK1/Cyclin B1*, *CDK4/Cyclin D*, *CDK2/Cyclin E*, *PLK1*, and *PLK4*), providing evidence for deregulated cell cycle machinery and cell division. Importantly, these key targets agree with those of ongoing clinical trials investigating CDK1 and PLK1 inhibitors (ribociclib, rocovitine, palbociclib, and volasertib) alone or in combination with standard chemotherapy for OC treatment [62]. Thus, p53 reactivation exhibits pleiotropic effects; among the most important effects is the simultaneous inhibition of multiple OC-relevant kinases.

Studies have linked functional loss of p53 to aneuploidy in vitro and In vivo [29, 63–65]. However, recent studies have suggested that the concurrent loss of p53 and p73 directly affects CIN in cancer cells [66–68]. Notably, both transcription factors exhibit shared target genes, among which *CDKN1A* (*p21*) is critical for the inhibition of CDK1 and CDK2. However, p21 contributes to cell cycle arrest in the G1 and G2 phases, and its absence introduces various mitotic aberrations in tumor cells [51, 69, 70]. Schmidt *et al.* [71] revealed that the inactivation of p53/p73 or the absence of p21 drives CIN in a CDK1-dependent manner. The loss of p21 unleashes CDK1 activity, leading to abnormal rates of microtubule assembly and subsequent CIN in cancer cells, which typically maintain CIN. Interestingly, our transcriptomic data revealed that restoring functional p53 led to significant upregulation of p73 and *CDKN1A* gene expression. Restoration of the p53/p73 and p21 axes proved sufficient to mitigate or at least partially reverse the observed CIN in surviving parental OVCAR-8 cancer

FIGURE 8 Intraperitoneal injection of OVCAR-8 cells followed by intraperitoneal treatment of mice with liposomal p53-mRNA prevents tumor formation and organ dissemination in a xenograft mouse model. (A) Bioluminescence imaging of luciferase-expressing metastatic OVCAR-8 cell-bearing mice upon treatment with liposomal p53-mRNA (upper panel). Approximately 2×10^6 OVCAR-8 cells stably expressing luciferase were i.p. injected followed by treatment with liposomal p53-mRNA for three weeks ($2 \times 5 \mu\text{g}$ liposomal p53-mRNA per week). The color scale represents p/sec/cm²/steradian. Tumor burden of control and liposomal p53-mRNA-treated nude mice determined weekly by bioluminescence over a period of 9 weeks (lower panel; $n = 8$). $*P < 0.05$, $**P < 0.01$, $***P < 0.001$. Wilcoxon test, unpaired and two-tailed. (B) Determination of the body weight over the entire observation period. (C) Inspection of peritoneal structures and organs for tumor dissemination following laparotomy. (D) Bioluminescence imaging of removed murine organs (control vs. p53-mRNA treatment). (E) Hematoxylin and eosin-stained representative sections of ovary enclosed by bursal peritoneum and fat pad (a, e), small intestine (b, f), colon (c, g) and fat/peritoneum (d, h) of mice ip injected with OVCAR-8 cells alone (control a-d) or followed by i.p. application of p53-mRNA (e-h). In the control group animals, prominent tumor cell aggregates are visible associated with serosal surfaces and fat (arrows in a-d) in contrast to the p53-mRNA-treated animals. Scale bars 300 μm . i.p., intraperitoneal.

cells and highlights the connection between these factors and CIN. Moreover, a recent report indicated that p53 activation enhances DNA replication efficiency, whereas its elimination impedes replication fork progression [72]. Interestingly, *MDM2*, a gene product induced by p53, also supports DNA replication even in p53-deficient cells, suggesting that sustained MDM2 expression is one of the mechanisms by which p53 prevents replicative stress [72]. Thus, in addition to its well-known role in eliminating damaged cells, p53 contributes to genome protection during S-phase by preventing the appearance of stalled or collapsed replication forks by preventing DNA damage during replication. Furthermore, cisplatin-induced apoptosis is enhanced by p73 overexpression [73, 74]. Therefore, IVT-p53-mRNA delivery can be used with carboplatin, a standard therapeutic agent for HGSOC patients [75]. Given the high rate of p53 mutations in HGSOC, restoring p53 function may make the cells more susceptible to carboplatin, providing an important treatment alternative for further investigation.

We tested 2 xenograft models and demonstrated a dose-dependent reduction in p53-mRNA during tumor growth. Dissemination of mock-transfected cells in our orthotopic model mirrored the dissemination in HGSOC cancer patients [76]. The p53-mRNA treatment prior to orthotopic injection hampered tumor cell growth in a dose-dependent manner within the ovaries and spread to the organs of the peritoneal cavity, demonstrating the efficacy of p53-mRNA under orthotopic conditions. The usefulness of p53-mRNA treatment was also corroborated in a second xenograft experiment in which HGSOC cells were directly administered to the peritoneal cavity. A significant advantage of intraperitoneal chemotherapy is that it prevents hepatotoxicity and allows the metabolism of cancer drugs. Upon intraperitoneal administration of liposomal p53-mRNA, a massive dose-dependent reduction in tumor cell growth and dissemination was observed. The absence of weight loss and detailed necropsy revealed no tissue damage, supporting the nontoxic behavior of p53-mRNA.

No approved drugs exist to restore functional p53 in cancer cells expressing mutant p53. Overcoming this challenge is crucial, particularly for HGSOC. However, p53 gene therapy failed in OC clinical trials [56] probably because of neutralizing antibodies against viral delivery systems and the dominant-negative effect of the endogenous mutant p53. To explore this aspect, a detailed analysis of p53 tetramers in cells treated with IVT-p53-mRNA should be the subject of future biochemical investigations. New-generation IVT-mRNAs with optimized translational efficacy, delivered as liposomal IVT-mRNA, show promise for bypassing these obstacles. The IVT-mRNA offers several advantages over DNA-based drugs, including a high transfection efficiency, no risk of insertional mutagenesis,

and functional activity without nuclear entry. However, the reactivation of p53 in cancer therapy faces certain hurdles. Off-target effects and immune responses pose risks requiring further detailed research. Long-term safety concerns, potential resistance, and ethical considerations must be addressed. Combating the evolution of cancer cell resistance remains challenging. Additionally, the costs and clinical efficacy across diverse cancer types and stages are complex. Overcoming these hurdles demands ongoing research, technological advancements, and rigorous clinical trials to ensure the safe and effective reactivation of tumor suppressor genes in cancer treatment. Nevertheless, this study supports IVT-mRNA as an attractive tool for reactivating p53 in susceptible cancers for effective cancer therapy.

5 | CONCLUSION

This study demonstrated the effectiveness of the reactivation of the *TP53* tumor suppressor gene in HGSOC by IVT mRNA. Liposomal IVT mRNA resulted in efficient and sustained expression of WT p53 and precise rescue of p53 function; thus, inhibiting cell proliferation in HGSOC cells, reducing chromosomal instability, and triggering cell death. In different mouse models, p53-mRNA treatment led to a dose-dependent reduction in tumor growth and dissemination within the peritoneal cavity. These findings suggested that IVT-mRNA-based approaches hold promise for reactivating p53 in cancer cells and may offer a valuable therapeutic option for HGSOC.

DECLARATIONS

AUTHOR CONTRIBUTIONS

Monika Raab and Klaus Strebhardt conceptualized the study. Monika Raab, Samuel Peña-Llopis, Mourad Sanhaji, Daniela Fitz, Monika Kressin, Sven Becker, and Klaus Strebhardt coordinated the study and wrote the manuscript. Monika Raab, Izabela Kostova, Samuel Peña-Llopis, Daniela Fitz, Monika Kressin, Seyed Mohsen Aberoumandi, Evelyn Ullrich, Mourad Sanhaji, and Klaus Strebhardt designed and performed experiments, interpreted results, and prepared figures. All the authors have read and approved the final version of the manuscript.

ACKNOWLEDGEMENTS

We are grateful to Prof. Franz Rödel (Department of Radiotherapy and Oncology, Goethe University, Frankfurt am Main, Germany), Prof. Florian Greten (Georg Speyer Haus, Frankfurt am Main, Germany), and Katja Stein (Children's Hospital, Department of Pediatrics, Experimental Immunology, Goethe University, Frankfurt am Main, Ger-

many) for supporting the animal experiments and Dr. Henner Farin (Georg Speyer Haus, Frankfurt am Main, Germany) for his help with OC organoid cultures. This work was supported by grants from the Deutsche Krebshilfe (70114007) and Wilhelm Sander Stiftung (Nr. 2021.023.1), German Cancer Consortium (DKTK), Heidelberg.

CONFLICT OF INTEREST STATEMENT

The authors declare no potential conflict of interest.

CONSENT FOR PUBLICATION

Not applicable.

ETHICS APPROVAL AND CONSENT TO PARTICIPATE

All tissues were obtained from patients who had undergone surgery at the University Hospital of Goethe University, with the consent of the patients and approval of the Goethe University Committee for Ethical Review of Research involving Human Subjects (approval number: SGO-1-2017). All the patients signed an informed consent form. All animal experiments were approved by the regional council of Darmstadt (V 54-19 c 18-FK/1128).

DATA AVAILABILITY STATEMENT

The data generated in this study are available from the corresponding author upon reasonable request.

ORCID

Samuel Peña-Llopis  <https://orcid.org/0000-0003-3847-1353>

Klaus Strebhardt  <https://orcid.org/0000-0003-2173-9763>

REFERENCES

- Luo Z, Wang Q, Lau WB, Lau B, Xu L, Zhao L, et al. Tumor microenvironment: The culprit for ovarian cancer metastasis? *Cancer Lett*. 2016;377(2):174–182.
- Yang Z, Wang W, Zhao L, Wang X, Gimple RC, Xu L, et al. Plasma cells shape the mesenchymal identity of ovarian cancers through transfer of exosome-derived microRNAs. *Sci Adv*. 2021;7(9):eabb0737.
- Bristow RE, del Carmen MG, Kaufman HS, Montz FJ. Radical oophorectomy with primary stapled colorectal anastomosis for resection of locally advanced epithelial ovarian cancer. *J Am Coll Surg*. 2003;17(4):565–574.
- Guppy AE, Nathan PD, Rustin GJ. Epithelial ovarian cancer: a review of current management. *Clin Oncol (R Coll Radiol)*. 2005;17(6):399–411.
- Wimberger P, Lehmann N, Kimmig R, Burges A, Meier W, Du Bois A, et al. Prognostic factors for complete debulking in advanced ovarian cancer and its impact on survival. An exploratory analysis of a prospectively randomized phase III study of the Arbeitsgemeinschaft Gynaekologische Onkologie Ovarian Cancer Study Group (AGO-OVAR). *Gynecol Oncol*. 2007;106(1):69–74.
- Garcia A, Singh H. Bevacizumab and ovarian cancer. *Ther Adv Med Oncol*. 2013;5(2):133–141.
- Lee JM, Ledermann JA, Kohn EC. PARP Inhibitors for BRCA1/2 mutation-associated and BRCA-like malignancies. *Ann Oncol*. 2014;25(1):32–40.
- Romero I, Bast RC, Jr. Minireview: human ovarian cancer: biology, current management, and paths to personalizing therapy. *Endocrinology*. 2012;153(4):1593–1602.
- Lane DP, Crawford LV. T antigen is bound to a host protein in SV40-transformed cells. *Nature*. 1979;278(5701):261–263.
- Alexandrova EM, Yallowitz AR, Li D, Xu S, Schulz R, Proia DA, et al. Improving survival by exploiting tumour dependence on stabilized mutant p53 for treatment. *Nature*. 2015;523(7560):352–356.
- Levine AJ, Oren M. The first 30 years of p53: growing ever more complex. *Nat Rev Cancer*. 2009;9(10):749–758.
- Biegging KT, Mello SS, Attardi LD. Unravelling mechanisms of p53-mediated tumour suppression. *Nat Rev Cancer*. 2014;14(5):359–370.
- Cancer Genome Atlas Research N. Integrated genomic analyses of ovarian carcinoma. *Nature*. 2011;474(7353):609–615.
- Bernardini MQ, Baba T, Lee PS, Barnett JC, Sfakianos GP, Secord AA, et al. Expression signatures of TP53 mutations in serous ovarian cancers. *BMC Cancer*. 2010;10:237.
- Bykov VJN, Eriksson SE, Bianchi J, Wiman KG. Targeting mutant p53 for efficient cancer therapy. *Nat Rev Cancer*. 2018;18(2):89–102.
- Sriraman A, Radovanovic M, Wienken M, Najafova Z, Li Y, Dobbstein M. Cooperation of Nutlin-3a and a Wip1 inhibitor to induce p53 activity. *Oncotarget*. 2016;7(22):31623–31638.
- Lehmann S, Bykov VJ, Ali D, Andren O, Cherif H, Tidefelt U, et al. Targeting p53 in vivo: a first-in-human study with p53-targeting compound APR-246 in refractory hematologic malignancies and prostate cancer. *J Clin Oncol*. 2012;30(29):3633–3639.
- Kreis NN, Sanhaji M, Kramer A, Sommer K, Rodel F, Strebhardt K, et al. Restoration of the tumor suppressor p53 by downregulating cyclin B1 in human papillomavirus 16/18-infected cancer cells. *Oncogene*. 2010;29(41):5591–5603.
- Joerger AC, Bauer MR, Wilcken R, Baud MGJ, Harbrecht H, Exner TE, et al. Exploiting Transient Protein States for the Design of Small-Molecule Stabilizers of Mutant p53. *Structure*. 2015;23(12):2246–2255.
- Yu X, Vazquez A, Levine AJ, Carpizo DR. Allele-specific p53 mutant reactivation. *Cancer Cell*. 2012;21(5):614–625.
- Floquet C, Deforges J, Rousset JP, Bidou L. Rescue of non-sense mutated p53 tumor suppressor gene by aminoglycosides. *Nucleic Acids Res*. 2011;39(8):3350–3362.
- Joerger AC, Fersht AR. The p53 Pathway: Origins, Inactivation in Cancer, and Emerging Therapeutic Approaches. *Annu Rev Biochem*. 2016;85:375–404.
- Liu DS, Duong CP, Haupt S, Montgomery KG, House CM, Azar WJ, et al. Inhibiting the system xC(-)/glutathione axis selectively targets cancers with mutant-p53 accumulation. *Nat Commun*. 2017;8:14844.
- Peng X, Zhang MQ, Conserva F, Hosny G, Selivanova G, Bykov VJ, et al. APR-246/PRIMA-1(MET) inhibits thioredoxin reductase 1 and converts the enzyme to a dedicated NADPH oxidase. *Cell Death Dis*. 2017;8(4):e2751.

25. Qin S, Tang X, Chen Y, Chen K, Fan N, Xiao W, et al. mRNA-based therapeutics: powerful and versatile tools to combat diseases. *Signal Transduct Target Ther*. 2022;7(1):166.
26. Sahin U, Kariko K, Tureci O. mRNA-based therapeutics—developing a new class of drugs. *Nat Rev Drug Discov*. 2014;13(10):759–780.
27. Uchida S, Kinoh H, Ishii T, Matsui A, Tockary TA, Takeda KM, et al. Systemic delivery of messenger RNA for the treatment of pancreatic cancer using polyplex nanomicelles with a cholesterol moiety. *Biomaterials*. 2016;82:221–228.
28. Zhang R, Men K, Zhang X, Huang R, Tian Y, Zhou B, et al. Delivery of a Modified mRNA Encoding IL-22 Binding Protein (IL-22BP) for Colon Cancer Gene Therapy. *J Biomed Nanotechnol*. 2018;14(7):1239–1251.
29. Bronder D, Tighe A, Wangsa D, Zong D, Meyer TJ, Wardenaar R, et al. TP53 loss initiates chromosomal instability in fallopian tube epithelial cells. *Dis Model Mech*. 2021;14(11):dmm049001.
30. McShane LM, Altman DG, Sauerbrei W, Taube SE, Gion M, Clark GM, et al. Reporting recommendations for tumor MARKer prognostic studies (REMARK). *Nat Clin Pract Urol*. 2005;2(8):416–422.
31. Matthess Y, Kappel S, Spankuch B, Zimmer B, Kaufmann M, Strebhardt K. Conditional inhibition of cancer cell proliferation by tetracycline-responsive, H1 promoter-driven silencing of PLK1. *Oncogene*. 2005;24(18):2973–2980.
32. Raab M, Kappel S, Kramer A, Sanhaji M, Matthess Y, Kurunci-Csacsko E, et al. Toxicity modelling of Plk1-targeted therapies in genetically engineered mice and cultured primary mammalian cells. *Nat Commun*. 2011;2:395.
33. Mergener S, Siveke JT, Pena-Llopis S. Monosomy 3 Is Linked to Resistance to MEK Inhibitors in Uveal Melanoma. *Int J Mol Sci*. 2021;22(13):6727.
34. Tseng J-C, Vasquez KO, Peterson JD, editors. Optical Imaging on the IVIS SpectrumCT System: General and Technical Considerations for 2 D and 3 D Imaging, 2015.
35. Bialkowska AB, Ghaleb AM, Nandan MO, Yang VW. Improved Swiss-rolling Technique for Intestinal Tissue Preparation for Immunohistochemical and Immunofluorescent Analyses. *J Vis Exp*. 2016(113):54161.
36. Spankuch-Schmitt B, Bereiter-Hahn J, Kaufmann M, Strebhardt K. Effect of RNA silencing of polo-like kinase-1 (PLK1) on apoptosis and spindle formation in human cancer cells. *J Natl Cancer Inst*. 2002;94(24):1863–1877.
37. Petitjean A, Mathe E, Kato S, Ishioka C, Tavtigian SV, Hainaut P, et al. Impact of mutant p53 functional properties on TP53 mutation patterns and tumor phenotype: lessons from recent developments in the IARC TP53 database. *Hum Mutat*. 2007;28(6):622–629.
38. Leroy B, Girard L, Hollestelle A, Minna JD, Gazdar AF, Soussi T. Analysis of TP53 mutation status in human cancer cell lines: a reassessment. *Hum Mutat*. 2014;35(6):756–765.
39. Mullany LK, Wong KK, Marciano DC, Katsonis P, King-Crane ER, Ren YA, et al. Specific TP53 Mutants Overrepresented in Ovarian Cancer Impact CNV, TP53 Activity, Responses to Nutlin-3a, and Cell Survival. *Neoplasia*. 2015;17(10):789–803.
40. Ikediobi ON, Davies H, Bignell G, Edkins S, Stevens C, O'Meara S, et al. Mutation analysis of 24 known cancer genes in the NCI-60 cell line set. *Mol Cancer Ther*. 2006;5(11):2606–2612.
41. Henningsen KM, Manzini V, Magerhans A, Gerber S, Dobbelsstein M. MDM2-Driven Ubiquitination Rapidly Removes p53 from Its Cognate Promoters. *Biomolecules*. 2021;12(1):22.
42. Mitra AK, Davis DA, Tomar S, Roy L, Gurler H, Xie J, et al. In vivo tumor growth of high-grade serous ovarian cancer cell lines. *Gynecol Oncol*. 2015;138(2):372–377.
43. Bhowmik S, Bhowmik S, Maiti K, Chakra A, Shahi P, Rajamannar T. Phase-I randomized trial of doxorubicin hydrochloride liposome injection versus Caelyx(R) in multiple myeloma. *Leuk Lymphoma*. 2018;59(6):1478–1481.
44. Tang Z, Feng W, Yang Y, Wang Q. Gemcitabine-loaded RGD modified liposome for ovarian cancer: preparation, characterization and pharmacodynamic studies. *Drug Des Devel Ther*. 2019;13:3281–3290.
45. Du M, Zhang S, Liu X, Xu C, Zhang X. Ploidy Status of Ovarian Cancer Cell Lines and Their Association with Gene Expression Profiles. *Biomolecules*. 2023;13(1):92.
46. Graf RP, Eskander R, Brueggeman L, Stupack DG. Association of Copy Number Variation Signature and Survival in Patients With Serous Ovarian Cancer. *JAMA Netw Open*. 2021;4(6):e2114162.
47. Delaney JR, Patel CB, Bapat J, Jones CM, Ramos-Zapatero M, Ortell KK, et al. Autophagy gene haploinsufficiency drives chromosome instability, increases migration, and promotes early ovarian tumors. *PLoS Genet*. 2020;16(1):e1008558.
48. McDermott JE, Arshad OA, Petyuk VA, Fu Y, Gritsenko MA, Clauss TR, et al. Proteogenomic Characterization of Ovarian HGSC Implicates Mitotic Kinases, Replication Stress in Observed Chromosomal Instability. *Cell Rep Med*. 2020;1(1):100004.
49. Roy S, Tomaszowski KH, Luzwick JW, Park S, Li J, Murphy M, et al. p53 orchestrates DNA replication restart homeostasis by suppressing mutagenic RAD52 and POLtheta pathways. *Elife*. 2018;7:e31723.
50. Liu Y, Parry JA, Chin A, Duensing S, Duensing A. Soluble histone H2AX is induced by DNA replication stress and sensitizes cells to undergo apoptosis. *Mol Cancer*. 2008;7:61.
51. Kreis NN, Sommer K, Sanhaji M, Kramer A, Matthess Y, Kaufmann M, et al. Long-term downregulation of Polo-like kinase 1 increases the cyclin-dependent kinase inhibitor p21(WAF1/CIP1). *Cell Cycle*. 2009;8(3):460–472.
52. Liu XS, Song B, Liu X. The substrates of Plk1, beyond the functions in mitosis. *Protein Cell*. 2010;1(11):999–1010.
53. Liu XS, Li H, Song B, Liu X. Polo-like kinase 1 phosphorylation of G2 and S-phase-expressed 1 protein is essential for p53 inactivation during G2 checkpoint recovery. *EMBO Rep*. 2010;11(8):626–632.
54. Arend RC, Londono-Joshi AI, Straughn JM, Jr., Buchsbaum DJ. The Wnt/beta-catenin pathway in ovarian cancer: a review. *Gynecol Oncol*. 2013;131(3):772–779.
55. Morgan RJ, Jr., Alvarez RD, Armstrong DK, Burger RA, Chen LM, Copeland L, et al. Ovarian cancer, version 2.2013. *J Natl Compr Canc Netw*. 2013;11(10):1199–1209.
56. Zeimet AG, Marth C. Why did p53 gene therapy fail in ovarian cancer? *Lancet Oncol*. 2003;4(7):415–422.
57. Lang F, Schrors B, Lower M, Tureci O, Sahin U. Identification of neoantigens for individualized therapeutic cancer vaccines. *Nat Rev Drug Discov*. 2022;21(4):261–282.

58. Tusup M, French LE, De Matos M, Gatfield D, Kundig T, Pascolo S. Design of in vitro Transcribed mRNA Vectors for Research and Therapy. *Chimia (Aarau)*. 2019;73(6):391–394.
59. Mantovani F, Collavin L, Del Sal G. Mutant p53 as a guardian of the cancer cell. *Cell Death Differ*. 2019;26(2):199–212.
60. Rodriguez OC, Choudhury S, Kolukula V, Vietsch EE, Catania J, Preet A, et al. Dietary downregulation of mutant p53 levels via glucose restriction: mechanisms and implications for tumor therapy. *Cell Cycle*. 2012;11(23):4436–4446.
61. Ventura A, Kirsch DG, McLaughlin ME, Tuveson DA, Grimm J, Lintault L, et al. Restoration of p53 function leads to tumour regression in vivo. *Nature*. 2007;445(7128):661–665.
62. Lin ZP, Zhu YL, Ratner ES. Targeting Cyclin-Dependent Kinases for Treatment of Gynecologic Cancers. *Front Oncol*. 2018;8:303.
63. Tomasini R, Mak TW, Melino G. The impact of p53 and p73 on aneuploidy and cancer. *Trends Cell Biol*. 2008;18(5):244–252.
64. Tarapore P, Fukasawa K. p53 mutation and mitotic infidelity. *Cancer Invest*. 2000;18(2):148–155.
65. Zhang M, Zhuang G, Sun X, Shen Y, Wang W, Li Q, et al. TP53 mutation-mediated genomic instability induces the evolution of chemoresistance and recurrence in epithelial ovarian cancer. *Diagn Pathol*. 2017;12(1):16.
66. Bunz F, Fauth C, Speicher MR, Dutriaux A, Sedivy JM, Kinzler KW, et al. Targeted inactivation of p53 in human cells does not result in aneuploidy. *Cancer Res*. 2002;62(4):1129–1133.
67. Ertych N, Stolz A, Stenzinger A, Weichert W, Kaulfuss S, Burfeind P, et al. Increased microtubule assembly rates influence chromosomal instability in colorectal cancer cells. *Nat Cell Biol*. 2014;16(8):779–791.
68. Melino G, De Laurenzi V, Vousden KH. p73: Friend or foe in tumorigenesis. *Nat Rev Cancer*. 2002;2(8):605–615.
69. Warfel NA, El-Deiry WS. p21WAF1 and tumorigenesis: 20 years after. *Curr Opin Oncol*. 2013;25(1):52–58.
70. Medema RH, Klompmaaker R, Smits VA, Rijkssen G. p21waf1 can block cells at two points in the cell cycle, but does not interfere with processive DNA-replication or stress-activated kinases. *Oncogene*. 1998;16(4):431–441.
71. Schmidt AK, Pudelko K, Boekenkamp JE, Berger K, Kschischo M, Bastians H. The p53/p73 - p21(CIP1) tumor suppressor axis guards against chromosomal instability by restraining CDK1 in human cancer cells. *Oncogene*. 2021;40(2):436–451.
72. Klusmann I, Rodewald S, Muller L, Friedrich M, Wienken M, Li Y, et al. p53 Activity Results in DNA Replication Fork Processivity. *Cell Rep*. 2016;17(7):1845–1857.
73. Al-Bahlani S, Fraser M, Wong AY, Sayan BS, Bergeron R, Melino G, et al. P73 regulates cisplatin-induced apoptosis in ovarian cancer cells via a calcium/calpain-dependent mechanism. *Oncogene*. 2011;30(41):4219–4230.
74. Kim KC, Jung CS, Choi KH. Overexpression of p73 enhances cisplatin-induced apoptosis in HeLa cells. *Arch Pharm Res*. 2006;29(2):152–158.
75. du Bois A, Luck HJ, Meier W, Adams HP, Mobus V, Costa S, et al. A randomized clinical trial of cisplatin/paclitaxel versus carboplatin/paclitaxel as first-line treatment of ovarian cancer. *J Natl Cancer Inst*. 2003;95(17):1320–1329.
76. Yeung TL, Leung CS, Yip KP, Au Yeung CL, Wong ST, Mok SC. Cellular and molecular processes in ovarian cancer metastasis. A Review in the Theme: Cell and Molecular Processes in Cancer Metastasis. *Am J Physiol Cell Physiol*. 2015;309(7):C444–C456.

SUPPORTING INFORMATION

Additional supporting information can be found online in the Supporting Information section at the end of this article.

How to cite this article: Raab M, Kostova I, Peña-Llopis S, Fietz D, Kressin M, Aberoumandi SM, et al. Rescue of p53 functions by in vitro-transcribed mRNA impedes the growth of high-grade serous ovarian cancer. *Cancer Commun*. 2024;44:101–126.
<https://doi.org/10.1002/cac2.12511>